Letter

Enhancing the Anticancer Activity of Attenuated *Listeria monocytogenes* by Cell Wall Functionalization with "Clickable" Doxorubicin

Irene Lepori,[&] Marta Roncetti,[&] Marianna Vitiello, Elisabetta Barresi, Raffaella De Paolo, Paolo Maria Tentori, Caterina Baldanzi, Melissa Santi, Monica Evangelista, Giovanni Signore, Lorena Tedeschi, Claudia Gravekamp, Francesco Cardarelli, Sabrina Taliani, Federico Da Settimo, M. Sloan Siegrist,* and Laura Poliseno*

Read Online

ACCESS | Metrics & More | Article Recommendations | Supporting Information

ABSTRACT: Among bacteria used as anticancer vaccines, attenuated *Listeria monocytogenes* (Lm^at) stands out, because it spreads from one infected cancer cell to the next, induces a strong adaptive immune response, and is suitable for repeated injection cycles. Here, we use click chemistry to functionalize the Lm^at cell wall and turn the bacterium into an "intelligent carrier" of the chemotherapeutic drug doxorubicin. Doxorubicin-loaded Lm^at retains most of its biological properties and, compared to the control fluorophore-functionalized bacteria, shows enhanced cytotoxicity against melanoma cells both in vitro and in a xenograft model in zebrafish. Our results show that drugs can be covalently loaded on the Lm^at cell wall and pave the way to the development of new two-in-one therapeutic approaches combining immunotherapy with chemotherapy.
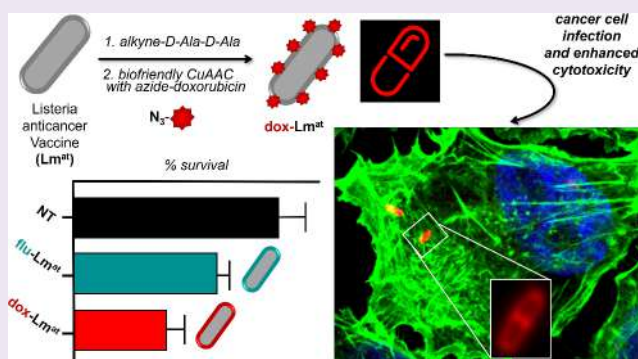
INTRODUCTION

Attenuated *Listeria monocytogenes* (Lm^at) has been widely investigated as an anticancer vaccine, because of its ability to trigger a strong and pleiotropic immune response against primary tumors, as well as metastases. In addition, it can spread from cell to cell, reaching even the deepest, most hypoxic tumor regions. Finally, Lm^at does not induce a strong antibody production; therefore, it is suitable for repeated injections.[1,2]

Due to its ability to selectively accumulate inside cancer tissues, Lm^at has been largely employed as a platform to deliver different kinds of therapeutic compounds inside the tumor mass.[3,4] The ease of genetic manipulation has enabled the use of this bacterium as a carrier for nucleic acids,[5] tumor-associated antigens (TAA),[6] and prodrug converting enzymes[7] with anticancer activity. In addition, there have been several successful attempts to combine Lm^at-mediated immunotherapy with chemotherapy.[8] The ability of Lm^at to deliver clinically relevant, nongenetically encoded molecules has also been exploited by our group, in the form of radiolabeling[9,10] and noncovalent surface coating of Lm^at with antibodies or immunomodulatory molecules.[9,11] Both strategies were safe for mice and therapeutically effective, leading to a stronger reduction of tumor burden and higher survival rates.

Several approaches have been developed to functionalize the surfaces of bacteria.[12−19] For Listeria, we and others have shown that the cell wall can be loaded via a combination of (i) metabolic labeling and (ii) bio-orthogonal click chemistry reaction.[20−22] Our two-step approach consists of (i) metabolic incorporation of azide- or alkyne-bearing D-Alanine probe in the peptidoglycan (PG) stem peptide, followed by (ii) covalent attachment of alkyne- or azide-bearing cargos through copper(I)-catalyzed azide−alkyne cycloaddition (CuAAC). This approach is highly efficient and, if properly tuned, it can be highly biocompatible.[23,24]

Here, we use click chemistry to covalently conjugate the chemotherapeutic drug doxorubicin to the Lm^at surface. Our approach has high loading efficiency, is bioorthogonal, and is amenable to both noncleavable and cancer cell-selective cleavable linkers. Having previously demonstrated the effectiveness of Lm^at against melanoma cells, both in vitro
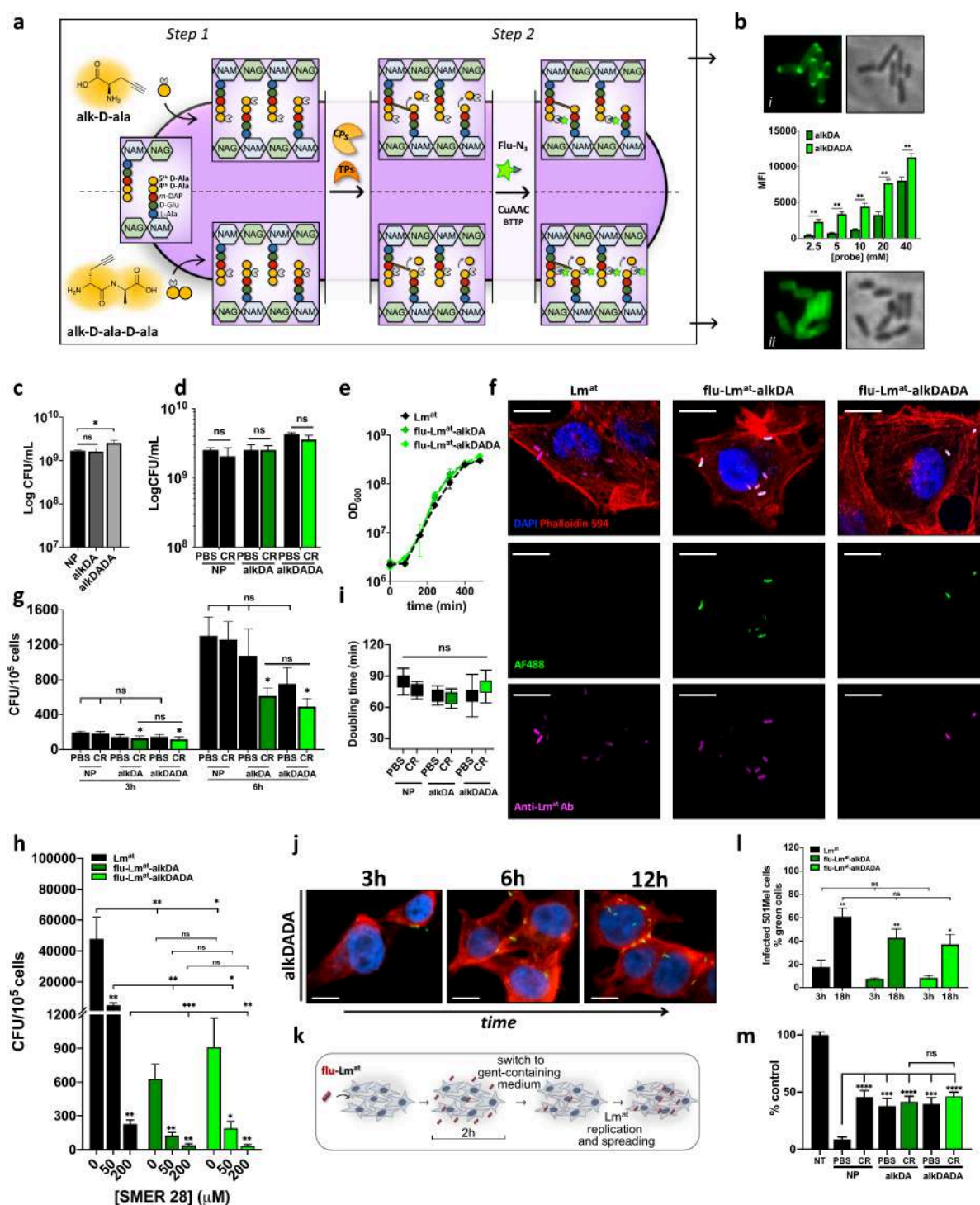
Figure 1. Generation of flu-Lm[at] and characterization of its biological features in melanoma cell lines. (a) Schematic representation of the two-step approach used to functionalize the Lm[at] cell wall. In the first step, Lm[at] is incubated with an alkyne-D-alanine probe (alkDA, upper) or an alkyne-D-alanine-D-alanine probe (alkDADA, lower), which result in the metabolic functionalization of the fifth or fourth D-alanine of the PG stem pentapeptide with an alkyne group, respectively. In the second step, the azide-bearing AF488 green fluorophore (az-AF488) is attached to bacterial cell wall via click reaction (CuAAC reaction, using BTTP as the ligand), so that fluorescent Lm[at] is obtained. When alkDA (but not alkDADA) is used, D,D-carboxypeptidases (CPs) and D,D-transpeptidases (TPs) can remove the alkyne- and/or fluorophore-bearing fifth D-alanine from the PG stem peptide, decreasing loading efficiency. TPs also cross-link the fourth d-alanine to meso-diaminopimelic acid (m-DAP), contributing to confer PG its characteristic 3D meshlike structure. (b) Fluorescence microscope images of bacteria incubated overnight (ON) with 1 mM alkDA probe (i, top) or alkDADA probe (ii, bottom), and MFI of bacteria populations incubated with increasing probe concentrations (middle). (c) Bacteria viability after ON incubation with 40 mM alkDA (dark gray bar) or alkDADA (gray bar) probe. (d) Viability of bacteria subjected to CuAAC reaction, after ON incubation with 40 mM alkDA probe (dark green bar) or alkDADA probe (green bar). For click reaction, the following optimized protocol was used: 25 μM az-AF488, 2.5 mM sodium ascorbate, 20 μM CuSO$_4$ and 160 μM BTTP, in PBS buffer, with incubation time set at 10 min (see Figure S4). (e) Proliferation of bacteria incubated ON with 40 mM alkDA or alkDADA probe and then subjected to CuAAC reaction with az-AF488 (flu-Lm[at]-alkDA, dark green line; flu-Lm[at]-alkDADA, green line). Unlabeled Lm[at] (not incubated with a probe nor

Figure 1. continued

subjected to CR) is taken as control (black line). Panels (f)−(h) show infectivity assays of AF488-loaded Lm[at]. (f) Representative confocal images of A375 melanoma cells after 3 h of infection with unlabeled Lm[at] (left), flu-Lm[at]-alkDA (middle), and flu-Lm[at]-alkDADA (right). Blue denotes DAPI staining of cell nucleus; red denotes staining of actin filaments using Phalloidin 594. Green denotes flu-Lm[at]-alkDA and flu-Lm[at]-alkDADA detected through AF488 green fluorophore. Pink represents a rendering of Lm[at] staining with primary anti-Listeria antibody and far-red secondary antibody. (g) A375 cells were infected at MOI 100 with bacteria incubated or not with alkDA probe or alkDADA probe and then subjected or not to click reaction. After 1 h of infection, extracellular Lm[at] was killed by medium replacement with fresh gentamycin-containing medium. At 3 h (left bars) and 6 h (right bars) post-infection, cells were lysed and intracellular Lm[at] was quantified by plating for CFU. (h) A375 cells were infected at MOI 100 with flu-Lm[at]-alkDA (dark green bars), flu-Lm[at]-alkDADA (green bars) or unlabeled Lm[at] (not incubated with a probe nor subjected to CR, black bars), in the presence of the indicated concentration of SMER28 inhibitor. After 2 h of infection, extracellular Lm[at] was killed by medium replacement with fresh gentamycin-containing medium. At 3 h post-infection, cells were lysed and intracellular Lm[at] was quantified by plating for CFU. Panels (i) and (j) show intracellular replication of AF488-loaded Lm[at]. (i) Bacteria doubling time between 3 h and 6 h was calculated based on the CFU obtained in panel (g). (j) Confocal microscope images of 501 Mel cells infected with flu-Lm[at]-alkDADA at MOI 100. After 1 h of infection, extracellular Lm[at] was killed by medium replacement with fresh gentamycin-containing medium. The fluorescence images are representative of the increase in the number of intracellular bacteria over time (3, 6, and 12 h post-infection). Legend: blue, DAPI staining of cell nucleus; red, staining of actin filaments using Phalloidin 594; green, flu-Lm[at]-alkDADA detected through AF488 green fluorophore. Panels (k) and (l) show cell-to-cell spreading assays. (k) Schematic representation of the experimental approach. 501 Mel melanoma cells were infected at MOI 50 with Cy5-loaded Lm[at]-alkDA or Lm[at]-alkDADA. After 2 h of infection, extracellular Lm[at] was killed by medium replacement with fresh gentamycin-containing medium. Then, infected cells were collected at 3 and 18 h post-infection, stained with anti-Listeria primary antibody and Alexa Fluor 488 secondary antibody, and analyzed by flow cytometry to determine the percentage of cells that acquire green fluorescence due to Lm[at] spreading. (l) Percentage of green 501 Mel cells at 18 vs 3 h post-infection with flu-Lm[at]-alkDA (dark green bars), flu-Lm[at]-alkDADA (green bars), or unlabeled Lm[at] (not incubated with a probe nor subjected to CR, black bars). (m) Kill rate assay. A375 melanoma cells were infected with AF488-loaded Lm[at]-alkDA or Lm[at]-alkDADA at MOI 2000. At 3 h post-infection, extracellular Lm[at] was killed by medium replacement with fresh gentamycin-containing medium. At 24 h post-infection, cells were fixed and stained with DAPI to count nuclei by fluorescence microscopy. [Legend: NP, no probe; PBS, no click reaction; CR, click reaction; CFU, colony forming units; MOI, multiplicity of infection; MFI, median fluorescence intensity. Graphs represent the mean ± SEM of at least three independent experiments, performed by using at least two independently functionalized stocks of Lm[at]. Unpaired t-test. (*) $p < 0.05$, (**) $p < 0.01$, (***) $p < 0.001$. ns: not statistically significant.]

and in the Braf/Pten melanoma model,[25] we chose melanoma as biological context and showed that doxorubicin-loaded Lm[at] has enhanced cytotoxicity against infected melanoma cells, compared to fluorophore-loaded control Lm[at].

Our loading method broadens the spectrum of tools for the chemical engineering of Lm[at] and sets up a versatile approach to covalently attach chemotherapeutic small molecules directly on its surface,[26,27] expanding the bacterium's utility as an anticancer vaccine.

■ RESULTS AND DISCUSSION

Biocompatible and Efficient Lm[at] Cell Wall Loading with a Fluorophore. The Listeria strain that we used for cell wall loading is XFL-7 Lm[at]-LLO (denoted as Lm[at], for the sake of brevity). This strain, which has been widely exploited by our research group as a vaccine against breast cancer,[11] pancreatic cancer[26] and melanoma,[25] is characterized by attenuated virulence due to the knockout of the Positive Regulatory Factor A (*prfA*) gene and its reintroduction as an episomal plasmid.[6]

Generation of a bacterium-drug conjugate for therapeutic purposes requires a loading process that is both efficient and able to preserve bacterial viability, ability to interact with host cells, and fitness. We opted for metabolic labeling of the amino acids that compose the stem peptide of PG, followed by covalent attachment of the drug of choice through a click chemistry reaction, because this is a controlled, site-specific approach that, contrary to nonspecific conjugation, allows one to predict and monitor the destiny of the payload. Furthermore, our approach can be adapted to ensure drug release in host cell cytoplasm once the bacterium reaches the tumor mass. The protocol for optimal loading of Lm[at] cell wall was set up using AF488 fluorophore as cargo.

We compared two of the most common click reactions: the strain-promoted azide−alkyne Cycloaddition (SPAAC)[27] and the copper(I)-catalyzed azide−alkyne Cycloaddition (CuAAC)

reactions.[28] In Figure S1, we show that, in our experimental setting, the CuAAC reaction is more efficient and able to preserve viability.[29,24] Then, we chose the commercially available alkyne-modified D-alanine (alkDA), which is expected to be incorporated into the fifth position of the peptidoglycan stem peptide, as a metabolic probe (Figure S2)[20] and azido-AF488 (az-AF488) as a fluorescent label. Finally, by tuning the components of CuAAC reaction (Figure S3), we established the optimal conditions to obtain AF488-Lm[at]-alkDA with maximal loading efficiency and, at the same time, no observable toxicity (Figure S4). We also observed that the optimized CuAAC reaction is not affected by Lm[at] genetic background (Figure S5).

Next, we aimed to overcome a crucial limitation of D-alanine probes in certain bacteria species including *L. monocytogenes*, namely their susceptibility to D,D-carboxypeptidases like penicillin binding protein 5 (Pbp5), which remove the fifth D-alanine of the stem peptide (Figures S6 and S7a−S7f).[20,30] We reasoned that a probe designed to install the chemical handle on the fourth D-alanine (instead of the fifth) of the PG stem peptide would be insensitive to Pbp5 activity and would increase PG loading efficiency (Figure S7g).[31] To this end, we resorted to the alkyne-D-alanine-D-alanine (alkDADA, also known as EDA-DA[31]) probe and compared it with the alkDA probe.[31] After confirming that both probes properly react with fluorophores containing an azido group (Figure S8a), we proceeded with Lm[at] loading with az-AF488 (Figure 1a). As expected, the loading increased at the increase of probe concentration and incubation time, yet the alkDADA probe yielded a loading that was consistently higher than that of alkDA (Figure 1b and Figure S8b). Neither probe was toxic for Lm[at], even after overnight (ON) incubation (Figure 1c), and neither bacteria viability nor proliferation were affected upon CuAAC reaction (see Figures 1d and 1e, as well as Figures S8c−S8g). Importantly, growing Lm[at] retains its cargo for

several generations, although fluorescence is inevitably diluted upon bacterial replication (Figure S8h).

We also investigated whether cell wall loading impacts fluorescent Lm[at] interaction with host cells, i.e., its ability to infect cancer cells, to spread from cell to cell, and to kill infected cells.

While AF488-loaded Lm[at] retained its ability to infect A375 melanoma cells (Figure 1f), AF488-loaded Lm[at] infection was less efficient than that of unlabeled Lm[at] (Figure 1g). To investigate this phenomenon further, we tested infectivity upon treatment with increasing concentrations of SMER28, a broad-spectrum inhibitor of *L. monocytogenes* penetration within cells.[32,2] Both unlabeled Lm[at] (Figure 1h, black bars) and AF488-loaded Lm[at] (Figure 1h, green bars) showed a dose-dependent reduction in cell penetration (compare 0 vs 50/200 μM SMER28), suggesting that the mechanism(s) used by Lm[at] to penetrate host cells are dampened but not fundamentally altered by cell wall functionalization. Nevertheless, once inside cancer cells, fluorescent Lm[at] replicates approximately at the same rate as unlabeled Lm[at] (Figures 1i and 1j). Although the exact mechanism responsible for the reduction in infectivity remains to be established, we speculate that cell wall functionalization may alter the deformability or accessibility of the heteropolymeric mesh and partially impair surface interactions between bacterial and cancer cells. Additionally, or alternatively, cell wall functionalization may interfere with Lm[at] protein localization.[33]

After endocytosis and phagosome-escape, Lm[at] spreads directly from the cytoplasm of one cell into the cytoplasm of another.[2] To test whether fluorophore loading affects this feature, we monitored the increase in the percentage of infected 501 Mel melanoma cells over time upon the removal of extracellular Lm[at] (Figure 1k). We conjugated Lm[at] with azido-Cy5 fluorophore (az-Cy5) and stained intracellular Lm[at] with anti-Lm antibody coupled with a secondary antibody labeled with AF488 fluorophore. Comparing 3 h and 18 h post-infection, we observed that the increase in the percentage of AF488-positive cells previously infected with unlabeled Lm[at] (black bars in Figure 1l) and Cy5-positive Lm[at] (green bars in Figure 1l) is similar. We also performed a direct monitoring of Cy5-positive bacteria-containing 501 Mel melanoma cells. As shown in Figure S9a, we observed that the percentage of such cells increases over time only in the case of the spreading-competent Cy5-Lm[at]-alkDA strain, not in the case of Cy5-Lm[at]-OVA-alkDA strain, which is avirulent, because of it being unable to escape the phagosome and, thus, spread cell to cell.[25] Finally, we observed that the increase over time in the percentage of Cy5-positive bacteria-containing cells has similar trend upon infection with Cy5-loaded Lm[at]-alkDA and Lm[at]-alkDADA (Figure S9b). All together, these results attest that fluorophore-loaded Lm[at] fully retains its ability to spread cell to cell.

The cytotoxicity exerted by fluorescent Lm[at] against melanoma cells was measured using a kill rate assay. AF488-loaded Lm[at] retained its ability to kill A375 cells, but cell wall functionalization has a negative impact on this biological feature, which becomes evident at high MOI (compare the results obtained with MOI 200 (Figure S9c) with those obtained with MOI 2000 (Figure 1m)). The lower cytotoxicity of AF488-loaded Lm[at]-alkDA and Lm[at]-alkDADA (green bars in Figure 1m) is consistent with their impaired infectivity (green bars in Figure 1g). However, bacteria only incubated with the probes (alkDA-PBS bar and alkDADA-PBS bar in

Figure 1m), or only subjected to the CuAAC reaction (NP-CR bar in Figure 1m), show reduced cytotoxicity as well. Although statistical significance is not reached, incubation with the two probes does decrease the infectivity (alkDA-PBS bar and alkDADA-PBS bar in Figure 1g, 6 h). This suggests that, when present in abundance within the cell wall, even the minor chemical modification represented by the alkyne group can affect Lm[at] biological properties, compromising its ability to interact with and later kill host cells. Conversely, the decreased cytotoxicity of Lm[at] only subjected to a click reaction might be a consequence of the presence of copper(I) in the reaction mix.

In summary, we carefully optimized metabolic labeling and CuAAC reaction to achieve high levels of Lm[at] cell wall loading without compromising bacterial viability and proliferation. However, a decrease in infectivity, with a consequent decrease in cytotoxicity, are observed. Given the superior loading efficiency compared to alkDA, we chose alkDADA probe to optimize bacterial cell wall loading with a drug. Therefore, in the experiments aimed at assessing the increased cytotoxicity of drug-loaded Lm[at], we used fluorophore-loaded Lm[at]-alkDADA as a control.

Doxorubicin Conjugation Increases Lm[at] Cytotoxicity against Melanoma Cells. The optimization of the two-step loading approach with fluorophores enabled precise and quantitative characterization of each variable involved in the cell wall loading of Lm[at]. However, the physicochemical properties of individual small molecules require some tailoring of the conjugation protocol. More specifically, the optimal conditions defined for the first step (i.e., the metabolic incorporation of the probe) can be applied irrespective of the chosen cargo, while the second step (i.e., the click reaction) requires small molecule-tailored optimization. Several characteristics of the chosen drug, such as water solubility, steric hindrance, and polarity, may in fact affect the accessibility of the azido-modified drug to the alkyne group embedded in the thick, meshlike layer of Gram-positive peptidoglycan.[34,35]

As a proof-of-concept drug to functionalize Lm[at], we chose doxorubicin (dox). This drug is well-known to cause cytotoxicity due to nuclear accumulation and DNA damage,[36] while its intrinsic red fluorescence facilitates the assessment of the efficiency of the functionalization process. We also investigated two different chemical linkers to attach doxorubicin onto the Lm[at] surface. The azidoacetic linker (Figure S10a) is small and uncleavable. It was chosen for its compact size, which is expected to minimize the steric hindrance and facilitate incorporation into the peptidoglycan mesh. The az-VC linker contains the azido group (az), a PEG$_4$ spacer attached to a Valine-Citrulline dipeptide (VC) and a self-immolative *para*-aminobenzyl carbamate (PABC) spacer (Figure S11a). Although longer and bulkier than the azidoacetic linker, the az-VC linker allows the specific cleavage of Valine-Citrulline dipeptide by Cathepsin proteases, which are overexpressed in cancer tissues.[37] This feature, together with the presence of the self-immolative spacer, is expected to enable release of native doxorubicin inside infected cells.[38]

First, we conjugated doxorubicin with the commercially available azidoacetic linker, obtaining az-dox (Figures S10b–S10d), while an az-VC linker conjugated with doxorubicin was purchased from a commercial source (az-VC-dox). Then, we tested the biological effects of the linker-dox conjugates on melanoma cells. We found that even the small 3′-N-modification on the aminoglycoside portion of the drug leads
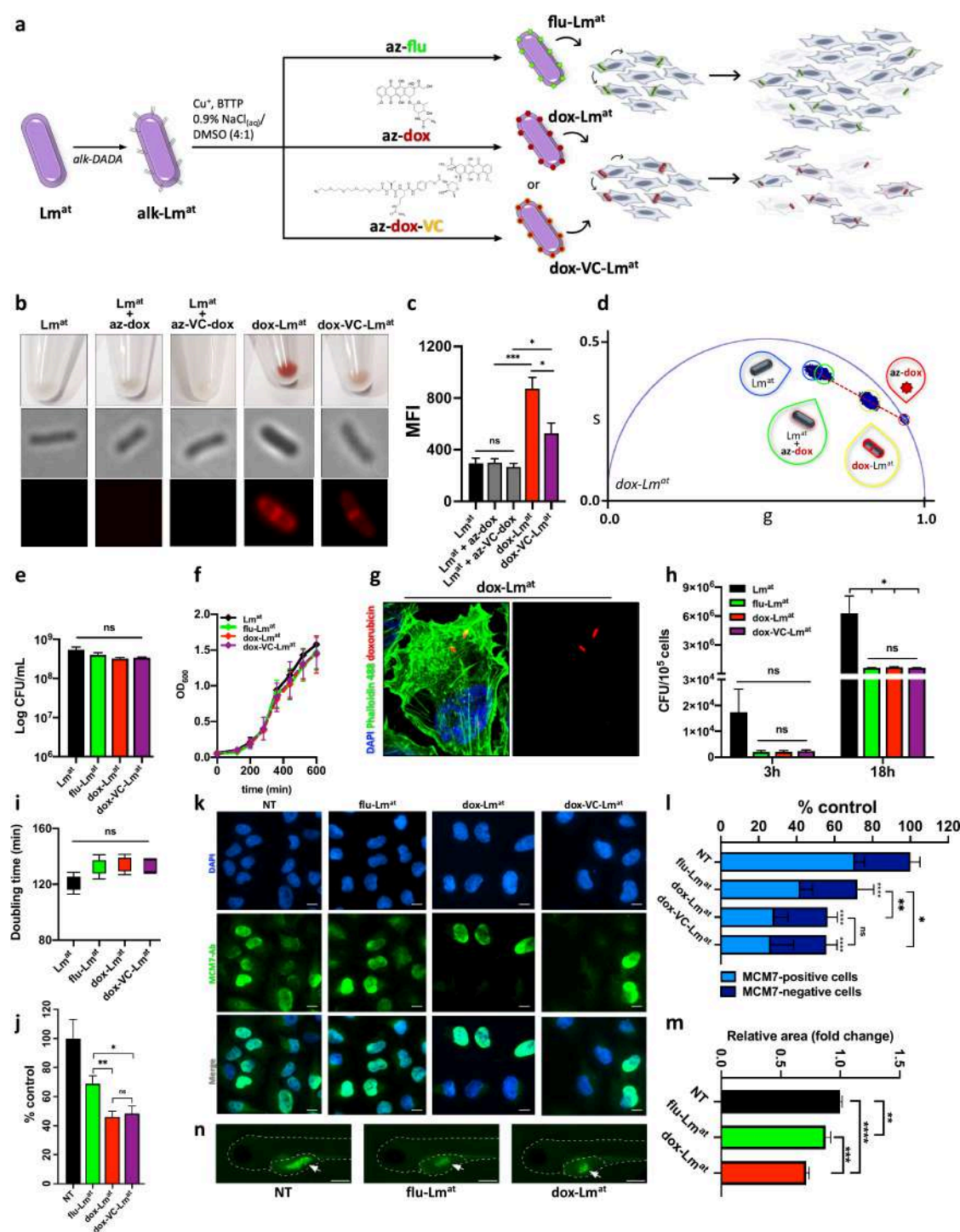
Figure 2. dox-Lm^{at} shows enhanced anticancer potential in melanoma cell lines. (a) Schematic representation of the experimental design used to functionalize Lm^{at} with doxorubicin and investigate whether dox-loaded Lm^{at} has enhanced cytotoxicity in vitro. Once preincubated with alkDADA, Lm^{at} is loaded with azide-bearing molecules (az-ATTO740 (az-flu), az-doxorubicin (az-dox) or az-VC-doxorubicin (az-VC-dox)) via CuAAC reaction to generate flu-Lm^{at}, dox-Lm^{at}, and dox-VC-Lm^{at}, respectively. For click reaction, the following optimized protocol was used: 5 μM az-ATTO740, 200 μM az-dox, or 200 μM az-VC-dox; 7.5 mM sodium ascorbate, 60 μM CuSO$_4$ and 480 μM BTTP; 0.9% w/v NaCl in water as reaction solvent; 25% DMSO as a cosolvent. After infection with flu-Lm^{at}, melanoma cells show decreased viability due to bacteria intrinsic cytotoxicity, which is enhanced when dox-Lm^{at} or dox-VC-Lm^{at} are used instead. (b) Pictures of bacterial cell pellets (top) and fluorescence microscope images (bottom) of: untreated Lm^{at}; Lm^{at} not metabolically labeled with the probe, but subjected to CuAAC reaction with az-dox (Lm^{at} + az-dox) or az-VC-dox (Lm^{at} + az-VC-dox); dox-Lm^{at}; dox-VC-Lm^{at}. (c) Quantification by flow cytometry of the MFI of the samples treated as in panel (b). (d) FLIM phasors plot of dox-Lm^{at}. The phasor populations of the different samples lie on different regions of the plot. From left to right: untreated Lm^{at} (blue teardrop); Lm^{at} not metabolically labeled with the probe but subjected to CuAAC reaction with az-dox (green teardrop); dox-Lm^{at} (yellow teardrop); az-dox (red teardrop). (e, f) Viability (panel (e)) and proliferation (panel (f)) of untreated Lm^{at} (black), flu-Lm^{at} (green), dox-Lm^{at} (red), and dox-VC-Lm^{at} (purple). Panels (g) and (h) show infectivity assays. (g) Representative confocal microscope images of A375 cells after 3 h of infection with dox-Lm^{at}. Blue denotes DAPI staining of cell nucleus. Green denotes staining of actin

Figure 2. continued

filaments using Phalloidin 488. Red denotes dox-Lm^{at}. (h) A375 cells were infected at MOI 100 with untreated Lm^{at} (black), flu-Lm^{at} (green) dox-Lm^{at} (red), and dox-VC-Lm^{at} (purple). After 2 h of infection, extracellular Lm^{at} was killed by medium replacement with fresh gentamycin-containing medium. At 3 h (left bars) and 18 h (right bars) post-infection, cells were lysed and intracellular Lm^{at} was quantified by plating for CFU. (i) Intracellular replication of bacteria. Bacteria doubling time between 3 h and 18 h was calculated based on the CFU obtained in (h) for Lm^{at} (black), flu-Lm^{at} (green), dox-Lm^{at} (red), and dox-VC-Lm^{at} (purple). (j) Kill rate assay. A375 melanoma cells were infected with flu-Lm^{at}, dox-Lm^{at} or dox-VC-Lm^{at} at MOI 2000. At 3 h post-infection, extracellular Lm^{at} was killed by medium replacement with fresh gentamycin-containing medium. At 48 h post-infection, cells were fixed and stained with DAPI to count nuclei by fluorescence microscopy. Panels (k) and (l) show the proliferation status of A375 melanoma cells infected with flu-Lm^{at}, dox-Lm^{at}, or dox-VC-Lm^{at} at MOI 1000. After 3 h post-infection, extracellular Lm^{at} was killed by medium replacement with fresh gentamycin-containing medium. At 48 h post-infection, cells were stained with anti-MCM7 antibody and proliferative vs nonproliferative cells were counted based on the presence vs absence of MCM7 nuclear staining. Representative microscope images (panel (k)) and quantification (panel (l)) of proliferative and nonproliferative A375 cells after infection with flu-Lm^{at}, dox-Lm^{at}, or dox-VC-Lm^{at}. Blue denotes DAPI; green denotes anti-MCM7 antibody. Panels (m) and (n) show the area of cancer cell mass developed in a xenograft model in zebrafish embryos. eGFP-expressing A375-PIG cells, previously infected with flu-Lm^{at} or dox-Lm^{at} at MOI 1000 for 2 h, were injected in 48 hpf embryos. [Here, and throughout, hpf stands for hours post-fertilization.] Then, embryos were allowed to grow for additional 48 h. At the end of this period, the area of green cancer cell mass was quantified. (m) Results of area quantification; at least 100 embryos were injected per experimental condition. (n) Representative pictures of 96 hpf embryos that, 48 h earlier, were injected with A375-PIG cells uninfected (left), infected with flu-Lm^{at} (middle), or infected with dox-Lm^{at} (right). The shape of the embryo and the perimeter of the injection site (yolk sac) are highlighted with a white dotted line, while the mass of cancer cells within the yolk sac (indicated with a white arrow) shows a green fluorescence signal. Scale bar = 300 μm. [Legend: NT, untreated cells; NP, no probe; PBS, no click reaction; CR, click reaction; CFU, colony forming units; MOI, multiplicity of infection; MFI, median fluorescence intensity. Graphs represent the mean $\pm$SEM of at least three independent experiments, performed by using at least two independently functionalized stocks of Lm^{at}.] Unpaired t-test (in vitro assays), Kruskal−Wallis test (Dunn's multiple comparisons test, xenograft assay). (*) $p < 0.05$, (**) $p < 0.01$, (***) $p < 0.001$, (****) $p < 0.0001$. ns, not statistically significant.]

to the loss of the ability of az-dox to accumulate inside nuclei (Figure S11b, compare panel iii with panel iv), with a consequent decrease in cytotoxicity (Figure S11c, compare the third and fourth bar). As expected, az-VC-dox was totally unable to accumulate in cell nuclei (Figure S11b, panel v) and showed an even lower cytotoxicity (Figure S11c, fifth bar). However, both nuclear localization and cytotoxicity were fully restored after incubation with acidified cell lysate containing active Cathepsins that cleave the VC linker and allow the release of doxorubicin in its native form (Figure S11b, panel vi and Figure S11c, sixth bar). As a further indication of Cathepsin-mediated release of native doxorubicin, az-VC-dox showed higher toxicity in SK-Mel-28 cells, which express Cathepsin B at higher levels, compared to A375 cells (Figures S11d and S11e).

We then proceeded with the optimization of Lm^{at} surface functionalization, tailored for the doxorubicin drug. First, we optimized experimental conditions such that the drug is not toxic for Lm^{at}. A long incubation under active replication conditions (30−120 min, 37 °C, BHI medium) is, in fact, toxic at doxorubicin concentrations as low as 20 μM (Figure 12a). However, a short incubation in the bacteriostatic conditions used for CuAAC reaction (10 min, RT, PBS buffer) is not associated with toxicity at doxorubicin concentrations as high as 500 μM (Figure S12b). Next, we addressed poor doxorubicin solubility/stability in a CuAAC reaction buffer (PBS, Figure S12c), which would severely impact efficiency and specificity of the conjugation with bacterial surface. We identified the physiological solution (0.9% w/v NaCl) as the best-performing reaction solvent (Figures S12d and S12e). Moreover, we found that a short incubation in the bacteriostatic conditions used for CuAAC reaction was not associated with toxicity using up to 40% dimethyl sulfoxide (DMSO) as a cosolvent (10 min, RT, PBS buffer, Figures S12f and S12g).

Overall, we defined the following as optimal reaction conditions that ensure maximal loading efficiency: 0.9% w/v NaCl solution as reaction solvent; 25% DMSO as a cosolvent; a 3-fold increase in click-reagent concentrations (7.5 mM

sodium ascorbate, 60 μM CuSO$_4$ and 480 μM BTTP), compared to the protocol used to obtain fluorescent Lm^{at}-alkDADA (2.5 mM sodium ascorbate, 20 μM CuSO$_4$ and 160 μM BTTP, see above); 200 μM az-dox or az-VC-dox (instead of 25 μM az-fluorophore).

Since our reaction conditions for doxorubicin loading were different from those used to load fluorophores, we reinvestigated bacterial physiology after cell wall functionalization with both the azidoacetic linker and the cleavable az-VC linker. dox-Lm^{at}-alkDADA and dox-VC-Lm^{at}-alkDADA were generated (denoted as dox-Lm^{at} and dox-VC-Lm^{at}, respectively, for the sake of brevity), while ATTO740-loaded Lm^{at}-alkDADA (flu-Lm^{at}, for the sake of brevity; see Figure 2a) was used as control. ATTO740 fluorophore was chosen for its excitation/emission spectrum that does not overlap with blue, green, and red fluorescence channels.

The effective conjugation of doxorubicin to Lm^{at} was detectable by eye, as a bacterial pellet color change (Figure 2b, top) and was confirmed by fluorescence microscopy (Figure 2b, bottom), flow cytometry (Figure 2c), and fluorescence lifetime imaging (FLIM, Figure 2d). In particular, the phasor approach to FLIM data allowed us to graphically assign a lifetime signature to any fluorescence species, including weak fluorophores like doxorubicin, and autofluorescent biological entities like bacteria.[39,40] Figure 2d shows the phasors plot of dox-Lm^{at} and related controls. As expected, the phasor population generated by dox-Lm^{at} (yellow teardrop) lies on the segment that connects the phasors of the two unconjugated species (namely, az-dox (red teardrop) and untreated Lm^{at} (blue teardrop)). In addition, when Lm^{at} is not metabolically labeled with the probe, but is still subjected to CuAAC reaction with az-dox, it generates a phasor population that lies very close to that of untreated Lm^{at} (green teardrop). This result strongly suggests that az-dox is conjugated to Lm^{at} via alkDADA, otherwise, unable to adsorb on Lm^{at}, it would be washed off as unreacted excess. Finally, we extracted doxorubicin from bacterial cell wall through enzymatic digestion with a mutanolysin/lysozyme mix and used a calibration curve to quantify the amount of drug loaded on

dox-Lm^{at} vs dox-VC-Lm^{at}. In agreement with visual inspection, fluorescence microscopy and flow cytometry, we found that the loading of dox-Lm^{at} is ∼10-fold higher than that of dox-VC-Lm^{at} (Figures S13a−S13c). By exposing dox-VC-Lm^{at} to acidified cell lysate containing active Cathepsins, we also confirmed that the VC-dox linker remains cleavable upon loading onto the Listeria cell wall (Figure S13d).

After verifying that dox-loaded Lm^{at} retains viability (Figure 2e) and proliferative activity (Figure 2f), we investigated its ability to infect A375 melanoma cells.

As expected, there was a significant reduction in infectivity, but it was comparable across bacteria loaded with all three different cargos (Figures 2g and 2h). The replication rate inside cancer cells was similar for Lm^{at} loaded with the three different cargos (Figure 2i).

To assess the anticancer potential of dox-loaded Lm^{at}, we performed a kill rate assay on A375 cells. As shown in Figure 2j, we found that infection with both dox-Lm^{at} and dox-VC-Lm^{at} causes a significant reduction in cell number, compared to flu-Lm^{at}. We also noticed that such a decrease is associated with a decrease in cell proliferation rather than an increase in dead cells. Therefore, we explored the replication state of infected cells by investigating the MCM7 protein. This well-known marker is recruited in the DNA replication machinery during active proliferation, and thus its localization switches from cytoplasmic to nuclear only in cells that are actively replicating.[41] As shown by microscope images (Figure 2k) and related quantitation (Figure 2l), A375 cells infected with both dox-Lm^{at} and dox-VC-Lm^{at} show a significantly lower percentage of replicating, MCM7-positive cells compared to the ones infected with flu-Lm^{at}.

We speculate that dox-Lm^{at} and dox-VC-Lm^{at} block melanoma cell proliferation at the same rate, despite the distinct strengths and weaknesses of the linkers. The small azidoacetic linker strongly favors Lm^{at} PG functionalization (Figure 2c) but lacks a release system for the native drug, leaving the fate of the drug attached to Lm^{at} surface to nonspecific mechanisms of drug release such as bacterial PG remodeling and host degradative enzymes.[42] As a consequence, doxorubicin conjugated to Lm^{at} via the azidoacetic linker is likely released in a 3′-N-modified form that cannot accumulate in cell nuclei (Figure S11b), hence its diminished toxic potential (Figures S11c and S11e). Conversely, the size of az-VC linker decreases conjugation efficiency (Figure 2c), but on the other hand ensures that the drug released inside melanoma cells is in its native form and can accumulate inside the nuclei (Figure S11b) and fully exert its cytotoxic potential (Figures S11c and S11e).

The anticancer potential of dox-loaded Lm^{at} was assessed in vivo as well, using a xenograft model in zebrafish. A375 cells previously infected with flu-Lm^{at} or dox-Lm^{at} at MOI 1000 were injected into the yolk sac of 48 hpf zebrafish embryos. [Note: hpf = hours post-fertilization.] Then, 48 h later, the tumor area was measured and, consistently with in vitro results, we found that dox-Lm^{at} is a stronger inhibitor of tumor growth, compared to flu-Lm^{at} (Figures 2m and 2n).

■ CONCLUDING REMARKS AND FUTURE PERSPECTIVES

The use of bacteria as immunotherapeutic agents has gained momentum in recent decades, mainly because these organisms can accumulate selectively in the cancer microenvironment but also because they are straightforward to manipulate and inexpensive. Therefore, immunotherapeutic bacteria are a sustainable option, especially for low-medium income countries.[43] With the aim to further increase their anticancer activity, bacteria have also been exploited as delivery platforms.[44,45] Many strategies have been developed that enable bacteria to express genetically encoded, therapeutically useful oligonucleotides, peptides, or proteins. Here, we develop a generalizable approach for functionalizing the surface of an immunotherapeutic bacterium with small molecules.

The Lm^{at} life cycle makes the organism a particularly attractive candidate for small-molecule functionalization. After host-cell-receptor-mediated endocytosis, the ability of Lm^{at} to escape the phagosome gives a great advantage to surface-attached small molecules, as they are delivered directly to the cytoplasm. Furthermore, cell-to-cell spreading allows the molecules not only to be selectively carried into the cancer microenvironment, but also to overcome the major barriers represented by the highly impermeable tumor mass, without relying on tumor vascularization, which is poor, and passive diffusion from one cell to another, which is slow and inefficient.[46] Finally, selective tropism for tumor sites is due to the fact that they are immunosuppressed, while it is independent of their genetic makeup. In other words, Lm^{at} does not need to be customized to reach a specific cancer type.[47−50]

The metabolic labeling/click chemistry protocol that we have refined here consists of two steps, which were both optimized, so that loading is maximized and, at the same time, viability and proliferation of loaded Lm^{at} are fully preserved: (i) the incorporation of alkDADA in peptidoglycan stem peptide; (ii) the covalent attachment of an azide-bearing cargo through CuAAC reaction. The two-step protocol enables robust cell wall incorporation (the alkyne reactive handle is compact and well-tolerated), as well as modular conjugation of any azide-bearing, small molecule with therapeutic potential. Furthermore, we showed that drug release in the cancer microenvironment can be enhanced by including a release system.

In light of the results obtained with noncovalently coated Lm^{at},[9,11] we expect that drug-loaded Lm^{at} is well-tolerated when systemically administered in vivo. Based on the fact that (i) in vitro, intracellular Lm^{at} shows persistent labeling and (ii) in vivo, it is carried by myeloid-derived suppressor cells (MDSCs),[51,26] reaching the tumor microenvironment within a few hours from injection,[9,25] we also assume that Lm^{at} will still be loaded with the drug when it gets to its intended destination. There, on-site drug release mechanisms (the physiological bacterial clearance and/or the action of intracellular as well as extracellular proteases) should enable specific and effective cancer cell targeting.[52] Since Lm^{at} does not trigger a strong humoral reaction (the small amount of antibody produced is not sufficient to protect against a reinfection[53]), we also speculate that the loaded bacterium is suitable for repeated injections that ensure steady drug delivery to the tumor microenvironment. Finally, the in vivo setting will allow us to appreciate the immunogenicity of loaded Lm^{at}, which is crucial to assess whether our approach indeed combines chemotherapy (doxorubicin) with immunotherapy (Lm^{at}). Interestingly, Lm^{at} itself is cytotoxic for cancer cells by causing ROS production,[25,54] while doxorubicin itself displays immunogenic properties.[55] Therefore, the cell-autonomous and noncell autonomous anticancer effects of dox-loaded Lm^{at} are expected to be highly pleiotropic and, hence, powerful.

In conclusion, our work describes a new approach for chemical engineering of the Lm^{at} surface and opens new possibilities for combination therapies in cancer treatment.

■ ASSOCIATED CONTENT

Ⓢⁱ Supporting Information

The Supporting Information is available free of charge at https://pubs.acs.org/doi/10.1021/acschembio.4c00250.

> Details regarding the setup of click reactions, the biological properties of loaded listeria, and the chemical and biological features of doxorubicin as cargo (Supplementary Figures 1−13). It also contains the description of all experimental protocols (Supplementary Methods). (PDF)

■ AUTHOR INFORMATION

Corresponding Authors

M. Sloan Siegrist − *Department of Microbiology, University of Massachusetts, Amherst, Massachusetts 01003-9316, United States; Molecular and Cellular Biology Graduate Program, University of Massachusetts, Amherst, Massachusetts 01003-9316, United States;* ⓘ orcid.org/0000-0002-8232-3246; Email: siegrist@umass.edu

Laura Poliseno − *Institute of Clinical Physiology, National Research Council (CNR-IFC), Pisa 56124, Italy; Oncogenomics Unit, Core Research Laboratory, ISPRO, Pisa 56124, Italy;* ⓘ orcid.org/0000-0001-6557-955X; Phone: +39 050 315 2780; Email: laura.poliseno@cnr.it, l.poliseno@ispro.toscana.it

Authors

Irene Lepori − *Institute of Clinical Physiology, National Research Council (CNR-IFC), Pisa 56124, Italy; Oncogenomics Unit, Core Research Laboratory, ISPRO, Pisa 56124, Italy;* Present Address: Present address for Irene Lepori: Department of Microbiology, University of Massachusetts, Amherst, MA 01003−9316, USA; ⓘ orcid.org/0000-0002-1602-0490

Marta Roncetti − *Institute of Clinical Physiology, National Research Council (CNR-IFC), Pisa 56124, Italy; Oncogenomics Unit, Core Research Laboratory, ISPRO, Pisa 56124, Italy; University of Siena, Siena 53100, Italy;* ⓘ orcid.org/0000-0003-0237-4359

Marianna Vitiello − *Institute of Clinical Physiology, National Research Council (CNR-IFC), Pisa 56124, Italy; Oncogenomics Unit, Core Research Laboratory, ISPRO, Pisa 56124, Italy;* Present Address: Present address for Marianna Vitiello: Genetics, Department of Biology, University of Pisa, Pisa 56126, Italy.; ⓘ orcid.org/0000-0001-7443-2728

Elisabetta Barresi − *Department of Pharmacy and CISUP-Center for Instrument Sharing, University of Pisa, Pisa 56126, Italy;* ⓘ orcid.org/0000-0002-9814-7195

Raffaella De Paolo − *Institute of Clinical Physiology, National Research Council (CNR-IFC), Pisa 56124, Italy; Oncogenomics Unit, Core Research Laboratory, ISPRO, Pisa 56124, Italy;* ⓘ orcid.org/0000-0002-9151-2866

Paolo Maria Tentori − *Center for Nanotechnology Innovation @NEST, Istituto Italiano di Tecnologia, Pisa 56126, Italy*

Caterina Baldanzi − *Institute of Clinical Physiology, National Research Council (CNR-IFC), Pisa 56124, Italy; Oncogenomics Unit, Core Research Laboratory, ISPRO, Pisa 56124, Italy*

Melissa Santi − *NEST-Scuola Normale Superiore, Istituto Nanoscienze, CNR (CNR-NANO), Pisa 56126, Italy;* ⓘ orcid.org/0000-0002-9374-883X

Monica Evangelista − *Institute of Clinical Physiology, National Research Council (CNR-IFC), Pisa 56124, Italy*

Giovanni Signore − *Fondazione Pisana per la Scienza ONLUS, Pisa 56017, Italy;* Present Address: Present address for Giovanni Signore: Department of Biology, University of Pisa, Pisa 56126, Italy.; ⓘ orcid.org/0000-0002-0067-2240

Lorena Tedeschi − *Institute of Clinical Physiology, National Research Council (CNR-IFC), Pisa 56124, Italy;* ⓘ orcid.org/0000-0002-8898-0888

Claudia Gravekamp − *Department of Microbiology and Immunology, Albert Einstein College of Medicine, New York, New York 10461, United States*

Francesco Cardarelli − *NEST-Scuola Normale Superiore, Istituto Nanoscienze, CNR (CNR-NANO), Pisa 56126, Italy;* ⓘ orcid.org/0000-0003-3049-5940

Sabrina Taliani − *Department of Pharmacy and CISUP-Center for Instrument Sharing, University of Pisa, Pisa 56126, Italy;* ⓘ orcid.org/0000-0001-8675-939X

Federico Da Settimo − *Department of Pharmacy and CISUP-Center for Instrument Sharing, University of Pisa, Pisa 56126, Italy;* ⓘ orcid.org/0000-0002-7897-7917

Complete contact information is available at: https://pubs.acs.org/10.1021/acschembio.4c00250

Author Contributions

&Authors I. Lepori and M. Roncetti made equal contributions to this work. I.L., M.S.S., and L.P. conceived the project; I.L., M.R., M.V., E.B., and L.P. designed the experiments; I.L., M.R., M.V., E.B., R.D.P., P.M.T., C.B., M.S., M.E., G.S., and L.T. performed the experiments and analyzed the data; C.G., F.C., S.T., F.D.S., M.S.S., and L.P. supervised the research; I.L., M.R., M.S.S., and L.P. wrote the manuscript with the help of all authors. The manuscript was discussed and approved by all authors.

Notes

The authors declare no competing financial interest.

■ ACKNOWLEDGMENTS

■ REFERENCES

(1) Flickinger, J. C., Jr.; Rodeck, U.; Snook, A. E. Listeria Monocytogenes as a Vector for Cancer Immunotherapy: Current Understanding and Progress. *Vaccines (Basel)* **2018**, 6 (3), 48.

(2) Radoshevich, L.; Cossart, P. Listeria Monocytogenes: Towards a Complete Picture of Its Physiology and Pathogenesis. *Nat. Rev. Microbiol* **2018**, 16 (1), 32−46.

(3) Forbes, N. S.; Coffin, R. S.; Deng, L.; Evgin, L.; Fiering, S.; Giacalone, M.; Gravekamp, C.; Gulley, J. L.; Gunn, H.; Hoffman, R. M.; Kaur, B.; Liu, K.; Lyerly, H. K.; Marciscano, A. E.; Moradian, E.; Ruppel, S.; Saltzman, D. A.; Tattersall, P. J.; Thorne, S.; Vile, R. G.; Zhang, H. H.; Zhou, S.; McFadden, G. White Paper on Microbial Anti-Cancer Therapy and Prevention. *J. Immunother. Cancer* **2018**, 6 (1), 78.

(4) Zhou, S.; Gravekamp, C.; Bermudes, D.; Liu, K. Tumour-Targeting Bacteria Engineered to Fight Cancer. *Nat. Rev. Cancer* **2018**, 18 (12), 727−743.

(5) van Pijkeren, J. P.; Morrissey, D.; Monk, I. R.; Cronin, M.; Rajendran, S.; O'Sullivan, G. C.; Gahan, C. G. M.; Tangney, M. A Novel *Listeria Monocytogenes* -Based DNA Delivery System for Cancer Gene Therapy. *Hum. Gene Ther.* **2010**, 21 (4), 405−416.

(6) Wood, L. M.; Paterson, Y. Attenuated Listeria Monocytogenes: A Powerful and Versatile Vector for the Future of Tumor Immunotherapy. *Front. Cell Infect. Microbiol.* **2014**, 4, 51.

(7) Stritzker, J.; Pilgrim, S.; Szalay, A. A.; Goebel, W. Prodrug Converting Enzyme Gene Delivery by *L. monocytogenes. BMC Cancer* **2008**, 8 (1), 94.

(8) Oladejo, M.; Paterson, Y.; Wood, L. M. Clinical Experience and Recent Advances in the Development of Listeria-Based Tumor Immunotherapies. *Front. Immunol.* **2021**, 12, No. 642316.

(9) Quispe-Tintaya, W.; Chandra, D.; Jahangir, A.; Harris, M.; Casadevall, A.; Dadachova, E.; Gravekamp, C. Nontoxic Radioactive Listeria(at) Is a Highly Effective Therapy against Metastatic Pancreatic Cancer. *Proc. Natl. Acad. Sci. U. S. A.* **2013**, 110 (21), 8668−8673.

(10) Chandra, D.; Selvanesan, B. C.; Yuan, Z.; Libutti, S. K.; Koba, W.; Beck, A.; Zhu, K.; Casadevall, A.; Dadachova, E.; Gravekamp, C. 32-Phosphorus Selectively Delivered by Listeria to Pancreatic Cancer Demonstrates a Strong Therapeutic Effect. *Oncotarget* **2017**, 8 (13), 20729−20740.

(11) Singh, M.; Quispe-Tintaya, W.; Chandra, D.; Jahangir, A.; Venkataswamy, M. M.; Ng, T. W.; Sharma-Kharkwal, S.; Carreno, L. J.; Porcelli, S. A.; Gravekamp, C. Direct Incorporation of the NKT-Cell Activator Alpha-Galactosylceramide into a Recombinant Listeria Monocytogenes Improves Breast Cancer Vaccine Efficacy. *Br. J. Cancer* **2014**, 111 (10), 1945−1954.

(12) Zoaby, N.; Shainsky-Roitman, J.; Badarneh, S.; Abumanhal, H.; Leshansky, A.; Yaron, S.; Schroeder, A. Autonomous Bacterial Nanoswimmers Target Cancer. *J. Controlled Release* **2017**, 257, 68−75.

(13) Xie, S.; Zhao, L.; Song, X.; Tang, M.; Mo, C.; Li, X. Doxorubicin-Conjugated Escherichia Coli Nissle 1917 Swimmers to Achieve Tumor Targeting and Responsive Drug Release. *J. Controlled Release* **2017**, 268, 390−399.

(14) Xie, S.; Chen, M.; Song, X.; Zhang, Z.; Zhang, Z.; Chen, Z.; Li, X. Bacterial Microbots for Acid-Labile Release of Hybrid Micelles to Promote the Synergistic Antitumor Efficacy. *Acta Biomater.* **2018**, 78, 198−210.

(15) Xie, S.; Xia, T.; Li, S.; Mo, C.; Chen, M.; Li, X. Bacteria-Propelled Microrockets to Promote the Tumor Accumulation and Intracellular Drug Uptake. *Chem. Eng. J.* **2020**, 392, No. 123786.

(16) Moreno, V. M.; Álvarez, E.; Izquierdo-Barba, I.; Baeza, A.; Serrano-López, J.; Vallet-Regí, M. Bacteria as Nanoparticles Carrier for Enhancing Penetration in a Tumoral Matrix Model. *Adv. Mater. Interfaces* **2020**, 7 (11), No. 1901942.

(17) Zheng, D.-W.; Chen, Y.; Li, Z.-H.; Xu, L.; Li, C.-X.; Li, B.; Fan, J.-X.; Cheng, S.-X.; Zhang, X.-Z. Optically-Controlled Bacterial Metabolite for Cancer Therapy. *Nat. Commun.* **2018**, 9 (1), 1680.

(18) Wu, F.; Liu, J. Decorated Bacteria and the Application in Drug Delivery. *Adv. Drug Delivery Rev.* **2022**, 188, No. 114443.

(19) Zeng, X.; Li, P.; Yan, S.; Liu, B.-F. Reduction/PH-Responsive Disassemblable MOF-Microbial Nanohybrid for Targeted Tumor Penetration and Synergistic Therapy. *Chem. Eng. J.* **2023**, 452, No. 139517.

(20) Siegrist, M. S.; Whiteside, S.; Jewett, J. C.; Aditham, A.; Cava, F.; Bertozzi, C. R. (D)-Amino Acid Chemical Reporters Reveal Peptidoglycan Dynamics of an Intracellular Pathogen. *ACS Chem. Biol.* **2013**, 8 (3), 500−505.

(21) Siegrist, M. S.; Aditham, A. K.; Espaillat, A.; Cameron, T. A.; Whiteside, S. A.; Cava, F.; Portnoy, D. A.; Bertozzi, C. R. Host Actin Polymerization Tunes the Cell Division Cycle of an Intracellular Pathogen. *Cell Rep.* **2015**, 11 (4), 499−507.

(22) Kelliher, J. L.; Grunenwald, C. M.; Abrahams, R. R.; Daanen, M. E.; Lew, C. I.; Rose, W. E.; Sauer, J.-D. PASTA Kinase-Dependent Control of Peptidoglycan Synthesis via ReoM Is Required for Cell Wall Stress Responses, Cytosolic Survival, and Virulence in Listeria Monocytogenes. *PLoS Pathog.* **2021**, 17 (10), No. e1009881.

(23) García-Heredia, A.; Pohane, A. A.; Melzer, E. S.; Carr, C. R.; Fiolek, T. J.; Rundell, S. R.; Lim, H. C.; Wagner, J. C.; Morita, Y. S.; Swarts, B. M.; Siegrist, M. S. Peptidoglycan Precursor Synthesis along the Sidewall of Pole-Growing Mycobacteria. *Elife* **2018**, 7, No. e37243.

(24) Yang, M.; Jalloh, A. S.; Wei, W.; Zhao, J.; Wu, P.; Chen, P. R. Biocompatible Click Chemistry Enabled Compartment-Specific PH Measurement inside *E. coli. Nat. Commun.* **2014**, 5 (1), 4981.

(25) Vitiello, M.; Evangelista, M.; Di Lascio, N.; Kusmic, C.; Massa, A.; Orso, F.; Sarti, S.; Marranci, A.; Rodzik, K.; Germelli, L.; Chandra, D.; Salvetti, A.; Pucci, A.; Taverna, D.; Faita, F.; Gravekamp, C.; Poliseno, L. Antitumoral Effects of Attenuated Listeria Monocytogenes in a Genetically Engineered Mouse Model of Melanoma. *Oncogene* **2019**, 38 (19), 3756−3762.

(26) Selvanesan, B. C.; Chandra, D.; Quispe-Tintaya, W.; Jahangir, A.; Patel, A.; Meena, K.; Alves Da Silva, R. A.; Friedman, M.; Gabor, L.; Khouri, O.; Libutti, S. K.; Yuan, Z.; Li, J.; Siddiqui, S.; Beck, A.; Tesfa, L.; Koba, W.; Chuy, J.; McAuliffe, J. C.; Jafari, R.; Entenberg, D.; Wang, Y.; Condeelis, J.; DesMarais, V.; Balachandran, V.; Zhang, X.; Lin, K.; Gravekamp, C. Listeria Delivers Tetanus Toxoid Protein to Pancreatic Tumors and Induces Cancer Cell Death in Mice. *Sci. Transl. Med.* **2022**, 14 (637), No. eabc1600.

(27) Lepori, I.; Oz, Y.; Im, J.; Ghosh, N.; Paul, M.; Schubert, U. S.; Fedeli, S. Bioorthogonal "Click" Cycloadditions: A Toolkit for Modulating Polymers and Nanostructures in Living Systems. *Reactions* **2024**, 5 (1), 231−245.

(28) Siegrist, M. S.; Swarts, B. M.; Fox, D. M.; Lim, S. A.; Bertozzi, C. R. Illumination of Growth, Division and Secretion by Metabolic Labeling of the Bacterial Cell Surface. *FEMS Microbiol. Rev.* **2015**, 39 (2), 184−202.

(29) Bird, R. E.; Lemmel, S. A.; Yu, X.; Zhou, Q. A. Bioorthogonal Chemistry and Its Applications. *Bioconjug. Chem.* **2021**, 32 (12), 2457−2479.

(30) Kuru, E.; Hughes, H. V.; Brown, P. J.; Hall, E.; Tekkam, S.; Cava, F.; de Pedro, M. A.; Brun, Y. V.; VanNieuwenhze, M. S. In Situ Probing of Newly Synthesized Peptidoglycan in Live Bacteria with Fluorescent D-Amino Acids. *Angew. Chem., Int. Ed.* **2012**, 51 (50), 12519−12523.

(31) Liechti, G. W.; Kuru, E.; Hall, E.; Kalinda, A.; Brun, Y. V.; VanNieuwenhze, M.; Maurelli, A. T. A New Metabolic Cell-Wall Labelling Method Reveals Peptidoglycan in Chlamydia Trachomatis. *Nature* **2014**, 506 (7489), 507−510.

(32) Kirchenwitz, M.; Stahnke, S.; Prettin, S.; Borowiak, M.; Menke, L.; Sieben, C.; Birchmeier, C.; Rottner, K.; Stradal, T. E. B.; Steffen, A. SMER28 Attenuates PI3K/MTOR Signaling by Direct Inhibition of PI3K P110 Delta. *Cells* **2022**, 11 (10), 1648.

(33) Rafelski, S. M.; Theriot, J. A. Mechanism of Polarization of Listeria Monocytogenes Surface Protein ActA. *Mol. Microbiol.* **2006**, *59* (4), 1262−1279.

(34) Ferraro, N. J.; Kim, S.; Im, W.; Pires, M. M. Systematic Assessment of Accessibility to the Surface of *Staphylococcus aureus*. *ACS Chem. Biol.* **2021**, *16* (11), 2527−2536.

(35) Kelly, J. J.; Dalesandro, B. E.; Liu, Z.; Chordia, M. D.; Ongwae, G. M.; Pires, M. M. Measurement of Accumulation of Antibiotics to *Staphylococcus aureus* in Phagosomes of Live Macrophages**. *Angew. Chem., Int. Ed.* **2024**, *63* (3), No. e202313870.

(36) Kciuk, M.; Gielecińska, A.; Mujwar, S.; Kołat, D.; Kałuzińska-Kołat, Ż.; Celik, I.; Kontek, R. Doxorubicin—An Agent with Multiple Mechanisms of Anticancer Activity. *Cells* **2023**, *12* (4), 659.

(37) Nejadmoghaddam, M.-R.; Minai-Tehrani, A.; Ghahremanzadeh, R.; Mahmoudi, M.; Dinarvand, R.; Zarnani, A.-H. Antibody-Drug Conjugates: Possibilities and Challenges. *Avicenna J. Med. Biotechnol.* **2019**, *11* (1), 3−23.

(38) McCombs, J. R.; Owen, S. C. Antibody Drug Conjugates: Design and Selection of Linker, Payload and Conjugation Chemistry. *AAPS J.* **2015**, *17* (2), 339−351.

(39) Caracciolo, G.; Palchetti, S.; Digiacomo, L.; Chiozzi, R. Z.; Capriotti, A. L.; Amenitsch, H.; Tentori, P. M.; Palmieri, V.; Papi, M.; Cardarelli, F.; Pozzi, D.; Laganà, A. Human Biomolecular Corona of Liposomal Doxorubicin: The Overlooked Factor in Anticancer Drug Delivery. *ACS Appl. Mater. Interfaces* **2018**, *10* (27), 22951−22962.

(40) Tentori, P.; Signore, G.; Camposeo, A.; Carretta, A.; Ferri, G.; Pingue, P.; Luin, S.; Pozzi, D.; Gratton, E.; Beltram, F.; Caracciolo, G.; Cardarelli, F. Fluorescence Lifetime Microscopy Unveils the Supramolecular Organization of Liposomal Doxorubicin. *Nanoscale* **2022**, *14* (25), 8901−8905.

(41) Dimitrova, D. S.; Berezney, R. The Spatio-Temporal Organization of DNA Replication Sites Is Identical in Primary, Immortalized and Transformed Mammalian Cells. *J. Cell Sci.* **2002**, *115* (21), 4037−4051.

(42) Radoshevich, L.; Cossart, P. Listeria Monocytogenes: Towards a Complete Picture of Its Physiology and Pathogenesis. *Nat. Rev. Microbiol.* **2018**, *16* (1), 32−46.

(43) Salicrup, L. A.; Ossandon, M.; Prickril, B.; Rasooly, A. Bugs as Drugs, Potential Self-Regenerated Innovative Cancer Therapeutics Approach for Global Health. *J. Glob. Health* **2020**, *10* (1), No. 010311.

(44) Lou, X.; Chen, Z.; He, Z.; Sun, M.; Sun, J. Bacteria-Mediated Synergistic Cancer Therapy: Small Microbiome Has a Big Hope. *Nanomicro. Lett.* **2021**, *13* (1), 37.

(45) Allemailem, K. S. Innovative Approaches of Engineering Tumor-Targeting Bacteria with Different Therapeutic Payloads to Fight Cancer: A Smart Strategy of Disease Management. *Int. J. Nanomed.* **2021**, *16*, 8159−8184.

(46) Azzi, S.; Hebda, J. K.; Gavard, J. Vascular Permeability and Drug Delivery in Cancers. *Front. Oncol.* **2013**, *3*, 211.

(47) MacDiarmid, J. A.; Mugridge, N. B.; Weiss, J. C.; Phillips, L.; Burn, A. L.; Paulin, R. P.; Haasdyk, J. E.; Dickson, K.-A.; Brahmbhatt, V. N.; Pattison, S. T.; James, A. C.; al Bakri, G.; Straw, R. C.; Stillman, B.; Graham, R. M.; Brahmbhatt, H. Bacterially Derived 400 Nm Particles for Encapsulation and Cancer Cell Targeting of Chemotherapeutics. *Cancer Cell* **2007**, *11* (5), 431−445.

(48) MacDiarmid, J. A.; Amaro-Mugridge, N. B.; Madrid-Weiss, J.; Sedliarou, I.; Wetzel, S.; Kochar, K.; Brahmbhatt, V. N.; Phillips, L.; Pattison, S. T.; Petti, C.; Stillman, B.; Graham, R. M.; Brahmbhatt, H. Sequential Treatment of Drug-Resistant Tumors with Targeted Minicells Containing SiRNA or a Cytotoxic Drug. *Nat. Biotechnol.* **2009**, *27* (7), 643−651.

(49) Sagnella, S. M.; Yang, L.; Stubbs, G. E.; Boslem, E.; Martino-Echarri, E.; Smolarczyk, K.; Pattison, S. L.; Vanegas, N.; St. Clair, E.; Clarke, S.; Boockvar, J.; MacDiarmid, J. A.; Brahmbhatt, H. Cyto-Immuno-Therapy for Cancer: A Pathway Elicited by Tumor-Targeted, Cytotoxic Drug-Packaged Bacterially Derived Nanocells. *Cancer Cell* **2020**, *37* (3), 354−370.e7.

(50) Kong, M.; D'Atri, D.; Bilotta, M. T.; Johnson, B.; Updegrove, T. B.; Gallardo, D. L.; Machinandiarena, F.; Wu, I.-L.; Constantino, M. A.; Hewitt, S. M.; Tanner, K.; Fitzgerald, D. J.; Ramamurthi, K. S. Cell-Specific Cargo Delivery Using Synthetic Bacterial Spores. *Cell Rep.* **2023**, *42* (1), No. 111955.

(51) Chandra, D.; Jahangir, A.; Quispe-Tintaya, W.; Einstein, M. H.; Gravekamp, C. Myeloid-Derived Suppressor Cells Have a Central Role in Attenuated Listeria Monocytogenes-Based Immunotherapy against Metastatic Breast Cancer in Young and Old Mice. *Br. J. Cancer* **2013**, *108* (11), 2281−2290.

(52) Mohamed, M. M.; Sloane, B. F. Multifunctional Enzymes in Cancer. *Nat. Rev. Cancer* **2006**, *6* (10), 764−775.

(53) Leong, M. L.; Hampl, J.; Liu, W.; Mathur, S.; Bahjat, K. S.; Luckett, W.; Dubensky, T. W.; Brockstedt, D. G. Impact of Preexisting Vector-Specific Immunity on Vaccine Potency: Characterization of *Listeria monocytogenes* -Specific Humoral and Cellular Immunity in Humans and Modeling Studies Using Recombinant Vaccines in Mice. *Infect. Immun.* **2009**, *77* (9), 3958−3968.

(54) Kim, S. H.; Castro, F.; Paterson, Y.; Gravekamp, C. High Efficacy of a Listeria-Based Vaccine against Metastatic Breast Cancer Reveals a Dual Mode of Action. *Cancer Res.* **2009**, *69* (14), 5860−5866.

(55) de Boo, S.; Kopecka, J.; Brusa, D.; Gazzano, E.; Matera, L.; Ghigo, D.; Bosia, A.; Riganti, C. INOS Activity Is Necessary for the Cytotoxic and Immunogenic Effects of Doxorubicin in Human Colon Cancer Cells. *Mol. Cancer* **2009**, *8* (1), 108.

SUPPORTING INFORMATION

Enhancing the anticancer activity of attenuated *Listeria monocytogenes* by cell wall functionalization with "clickable" doxorubicin

Irene Lepori[1,2,&,£], Marta Roncetti[1,2,3,&], Marianna Vitiello[1,2,#], Elisabetta Barresi[4,5], Raffaella De Paolo[1,2], Paolo Maria Tentori[6], Caterina Baldanzi[1,2], Melissa Santi[7], Monica Evangelista[1], Giovanni Signore[8,$], Lorena Tedeschi[1], Claudia Gravekamp[9], Francesco Cardarelli[7], Sabrina Taliani[4,5], Federico Da Settimo[4,5], M. Sloan Siegrist[10,11,*], Laura Poliseno[1,2,*]

[1]*Institute of Clinical Physiology, National Research Council (CNR-IFC), Pisa, 56124, Italy*

[2]*Oncogenomics Unit, Core Research Laboratory, ISPRO, Pisa, 56124, Italy*

[3]*University of Siena, Siena, 53100, Italy*

[4]*Department of Pharmacy, University of Pisa, Pisa, 56126, Italy*

[5]*CISUP-Center for Instrument Sharing, University of Pisa, Pisa, 56126, Italy*

[6]*Center for Nanotechnology Innovation @NEST, Istituto Italiano di Tecnologia, Pisa, 56126, Italy*

[7]*NEST-Scuola Normale Superiore, Istituto Nanoscienze, CNR (CNR-NANO), Pisa, 56126, Italy*

[8]*Fondazione Pisana per la Scienza ONLUS, San Giuliano Terme, 56017, Pisa, Italy*

[9]*Department of Microbiology and Immunology, Albert Einstein College of Medicine, New York, 10461, USA*

[10]*Department of Microbiology, University of Massachusetts, Amherst, 01003-9316, USA*

[11]*Molecular and Cellular Biology Graduate Program, University of Massachusetts, Amherst, 01003-9316, USA*

[&]equal contribution

*Corresponding authors:

Laura Poliseno, PhD
Oncogenomics Unit
Core Research Laboratory (CRL), ISPRO
Institute of Clinical Physiology (IFC), CNR
Via Moruzzi 1
56124 Pisa, Italy
Phone: +39 050 315 2780
Email: laura.poliseno@cnr.it, l.poliseno@ispro.toscana.it

M. Sloan Siegrist, PhD
Department of Microbiology
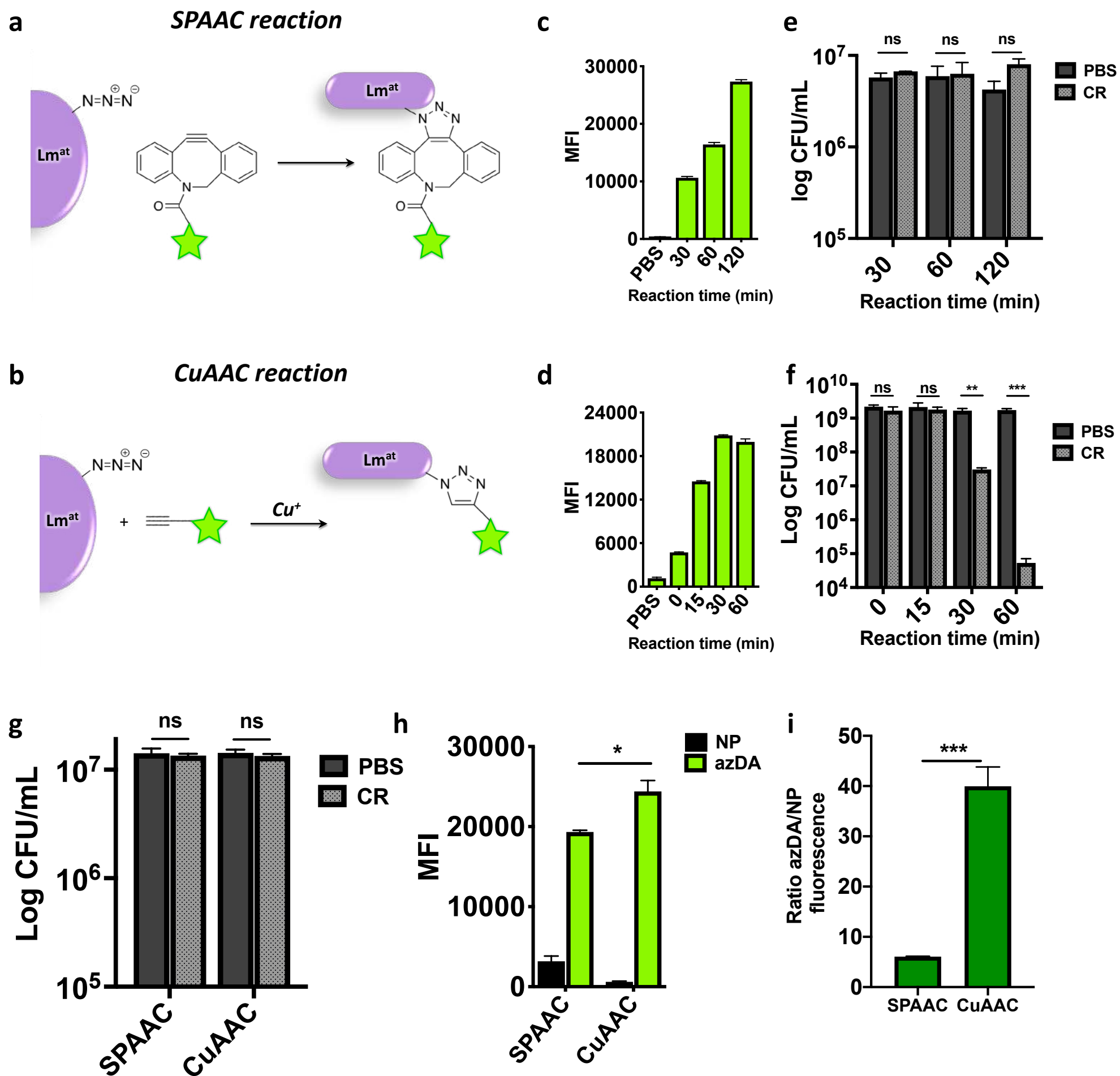418 Morrill Science Center IVN
University of Massachusetts
639 North Pleasant Street
Amherst, MA 01003-9298
Email: siegrist@umass.edu

Fig 1

Supplementary Figure 1. Comparison of SPAAC and CuAAC reactions in terms of fluorescence intensity and viability of fluorescent Lm^{at}.
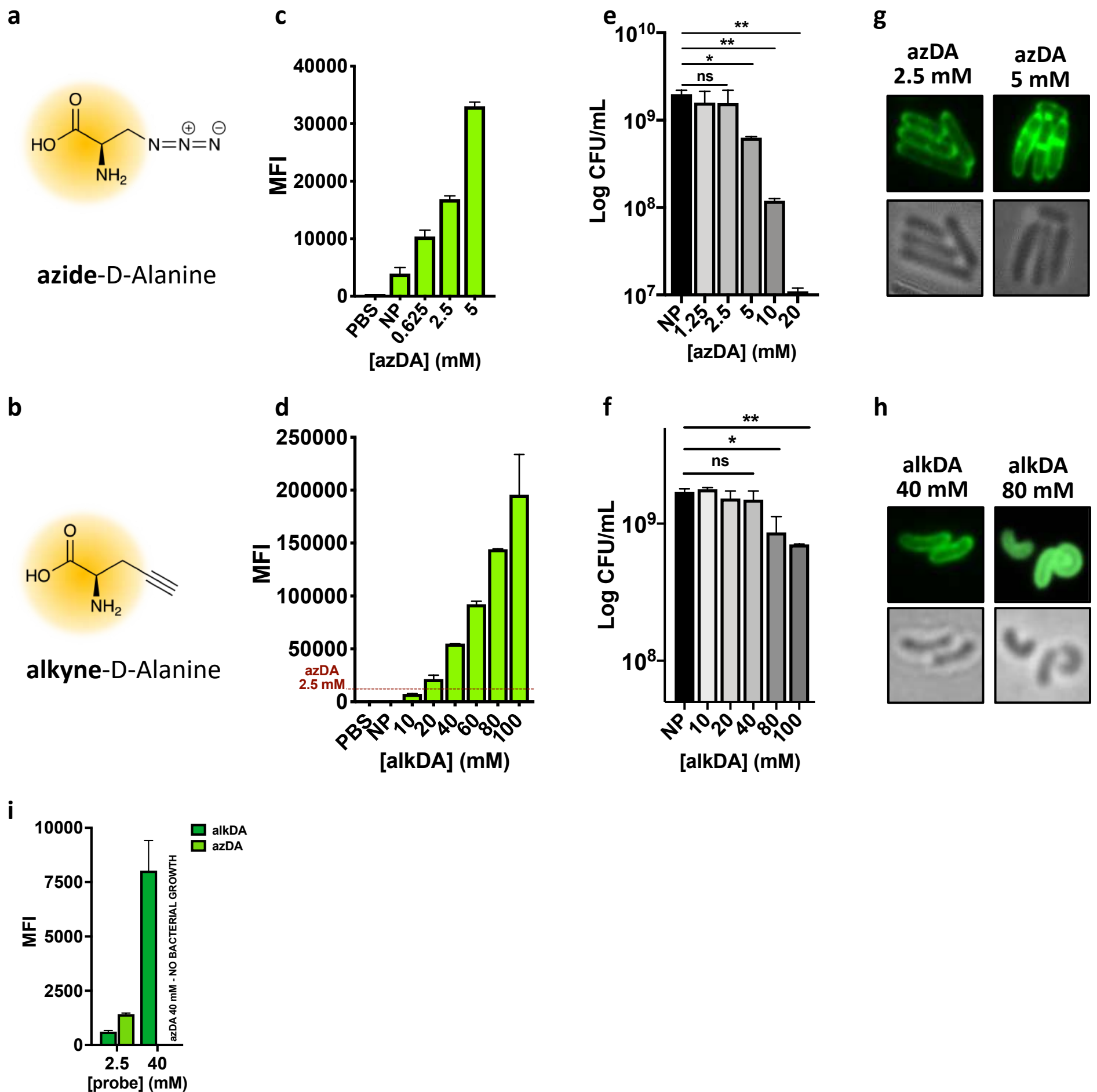
Loading efficiency was determined by flow cytometry analysis in terms of median fluorescence intensity (MFI), while toxicity was assessed by plating bacteria for colony forming units (CFU). Panels (**a**) and (**b**) show the chemical details of SPAAC and CuAAC reactions occurring on bacteria surface. In both cases, bacteria were metabolically labelled by overnight (ON) incubation with 2.5mM azDA probe. Then, click reaction was performed with alkyne-bearing AF488 green fluorophore as reaction partner.

(**c-f**) Establishment of the longest reaction time that is not toxic for bacteria, i.e. does not affect their viability. At the increase of incubation time, loading efficiency increases for both reactions (panel (**c**) and (**d**)). However, bacteria viability is preserved only in the case of SPAAC reaction (compare panel (**e**) and (**f**)).

(**g-i**) Comparison of loading efficiency at the longest reaction time that does not impair bacteria viability. At 60min reaction time for SPAAC and 15min reaction time for CuAAC, bacteria viability is totally preserved (**g**), while the loading efficiency is higher for CuAAC compared with SPAAC (**h**). This result becomes even more evident when the fluorescence acquired by bacteria upon click reaction is expressed as ratio over background (**i**).

NP: no probe; CR: click reaction (SPAAC or CuAAC depending on the graph).

Graphs show the mean±SEM of one experiment (three technical replicates), representative of three biological replicates. Unpaired t-test. *p < 0.05, **p < 0.01, ***p < 0.001. ns: not significant.

Fig 1

a

azide-D-Alanine

b

alkyne-D-Alanine

c

MFI

[azDA] (mM): PBS, NP, 0.625, 2.5, 5

d

MFI

azDA 2.5 mM

[alkDA] (mM): PBS, NP, 10, 20, 40, 60, 80, 100

e

Log CFU/mL

ns * ** **

[azDA] (mM): NP, 1.25, 2.5, 5, 10, 20

f

Log CFU/mL

ns * **

[alkDA] (mM): NP, 10, 20, 40, 80, 100

g

azDA 2.5 mM   azDA 5 mM

h

alkDA 40 mM   alkDA 80 mM

i

MFI

alkDA
azDA

azDA 40 mM - NO BACTERIAL GROWTH

[probe] (mM): 2.5, 40

Supplementary Figure 2. Comparison of azido-D-Alanine and alkyne-D-Alanine probes in terms of fluorescence intensity and viability of fluorescent Lm[at].

Bacteria were metabolically labelled by ON incubation with azide-D-Alanine (azDA) (**a**) or alkyne-D-Alanine (alkDA) (**b**) probe. We opted for ON incubation to maximize the number of chemical handles available on Lm[at] surface. Then, CuAAC reaction was performed with alk-AF488 or az-AF488 green fluorophore as reaction partner. Loading efficiency was determined by flow cytometry analysis in terms of median fluorescence intensity (MFI), while toxicity was assessed by plating bacteria for colony forming units (CFU).

For both probes, the increase in concentration results in increased loading efficiency (**c** and **d**), but it is also associated with decreased bacteria viability (**e** and **f**) and altered bacteria shape (**g** and **h**). azDA toxicity is stronger than that of alkDA, starting at 5mM (**e**), vs 80mM (**f**). The direct comparison of the highest non-toxic concentration for each probe (2.5mM for azDA and 40mM for alkDA, **i**) highlights that 2.5mM azDA probe leads to a higher fluorescence intensity compared to 2.5mM alkDA, but when the two probes are used at 40mM, the fluorescence intensity obtained with alkDA is higher than the one obtained with both probes at 2.5mM, while no bacterial growth is observed for azDA. NP: no probe.

Graphs show the mean±SEM of one experiment (three technical replicates), representative of three biological replicates. Unpaired t-test. *$p < 0.05$, **$p < 0.01$. ns: not significant.

Fig 1
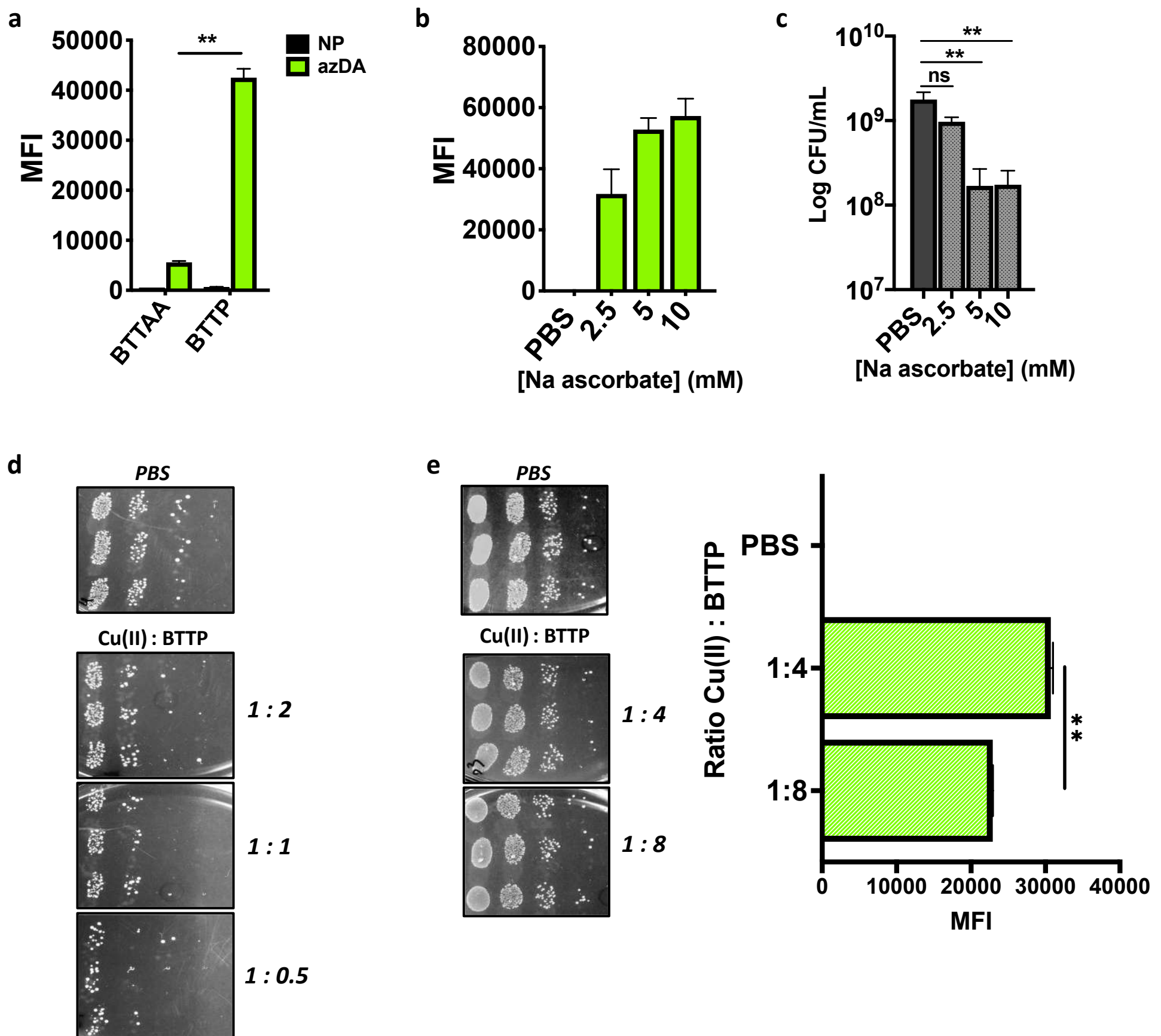
Supplementary Figure 3. Influence of CuAAC reaction components on fluorescence intensity and viability of fluorescent Lm[at].

Loading efficiency was determined by flow cytometry analysis in terms of median fluorescence intensity (MFI), while toxicity was assessed by plating bacteria for colony forming units (CFU).
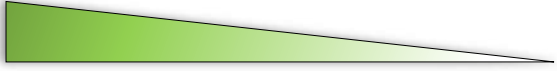
(**a**) Comparison between BTTAA and BTTP as ligands. Bacteria were metabolically labelled with 2.5mM azDA probe, then alk-AF488 fluorophore was used as partner in the click reaction. The higher MFI indicates that BTTP ligand is superior at co-catalyzing CuAAC reaction, compared to BTTAA.

(**b-c**) Establishment of the optimal concentration of sodium ascorbate in the reaction mix. MFI (**b**) and viability (**c**) of Lm[at] metabolically labelled with 40mM alkDA probe and then subjected to CuAAC reaction with az-AF488 fluorophore, using the indicated concentrations of sodium ascorbate in the reaction mix. Increasing the concentration of this salt, the loading efficiency increases, but viability decreases, probably due to the generation of increasingly high levels of Cu(I), the reduced toxic form of copper. The maximal concentration tolerated is 2.5mM.

(**d-e**) Establishment of the optimal CuSO_4:BTTP ratio in the reaction mix. Lm[at] was metabolically labelled with 40mM alkDA probe and then subjected to CuAAC reaction with az-AF488 fluorophor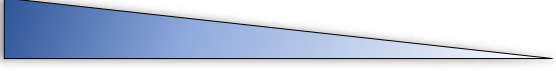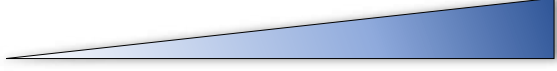e. The concentration of CuSO_4 in the reaction mix was kept constant at 20µM (taken as 1), while that of BTTP was varied between 10µM (taken as 0.5) and 160µM (taken as 8). (**d**) Bacteria viability is strongly affected at low BTTP concentrations (1:0.5, 1:1 and 1:2 ratios), while it is unaffected at high BTTP concentrations, which seem to protect from copper toxicity (1:4 and 1:8 ratios, **e, left**). If fluorescence intensity is considered as well (**e, right**), 1:4 ratio results the optimal one.

NP: no probe.

Graphs show the mean±SEM of one experiment (three technical replicates), representative of three biological replicates. Unpaired t-test. **p < 0.01. ns: not significant.

Fig 1

	Loading efficiency	Bacterial fitness
Click Reaction Incubation Time (min)	0 ▱ 60	0 ▰ 60
[Probe] (mM)	*azDA* 1.25 ▱ 20 *alkDA* 10 ▱ 100	*azDA* 1.25 ▰ 20 *alkDA* 10 ▰ 100
[Na Ascorbate] (mM)	2.5 ▱ 10	2.5 ▰ 10
CuSO₄ : BTTP Molar ratio	1 : 0.5 ▰ 1 : 8	1 : 0.5 ▱ 1 : 8

Supplementary Figure 4. Summary of the impact of click reaction conditions on loading efficiency and fitness of fluorescent Lm[at].

For all the investigated factors, the increase in loading efficiency is associated with a decrease in fitness (shape, viability, and proliferative activity) and *vice versa*. In the final protocol, we further optimized all the abovementioned factors, in order to achieve maximum loading efficiency without impairing bacteria fitness. Specifically, in the first step, Lm[at] cell wall is metabolically labelled by ON incubation with 40mM alkDA. In the second step, the azide-bearing AF488 green fluorophore (25µM az-AF488) is attached to the cell wall *via* a CuAAC reaction composed of metabolically labelled bacteria at 7.5×10^8 CFU/mL, 2.5mM sodium ascorbate, 20µM $CuSO_4$ and 160µM BTTP, in PBS buffer, with incubation time set at 10min.

Fig 1

a

b
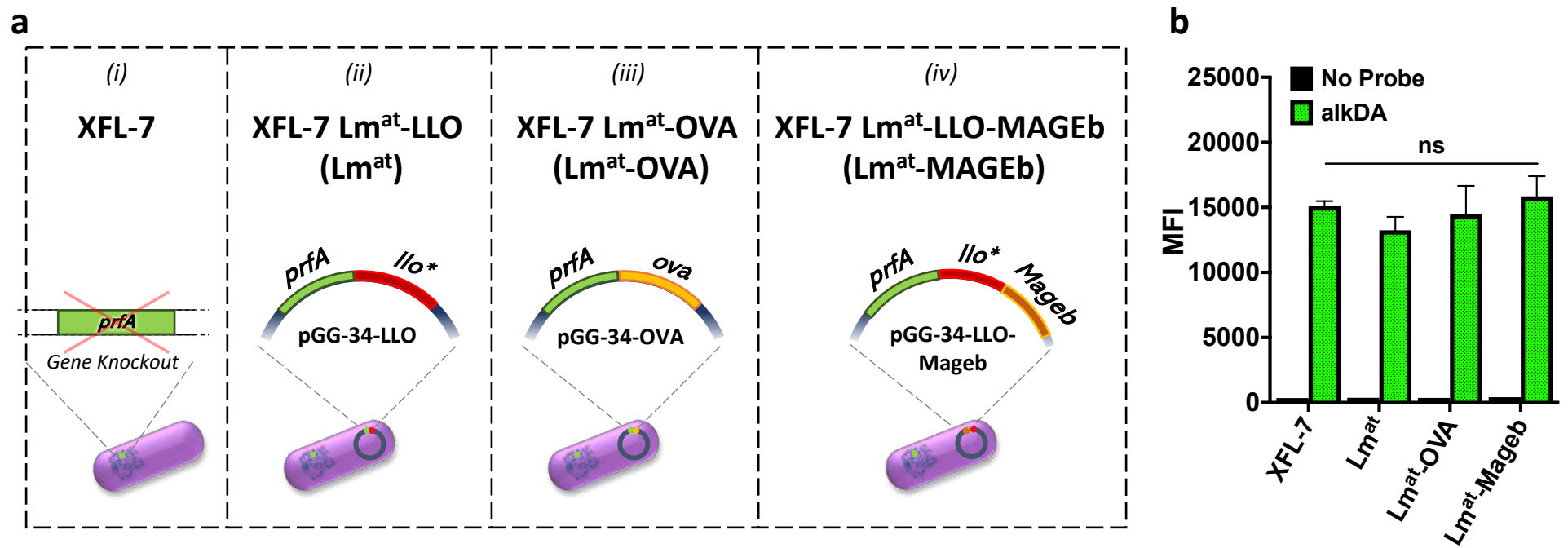
Supplementary Figure 5. The functionalization of Lm^at is not affected by genetic background.

(**a**) Strains of attenuated *Listeria monocytogenes* subjected to functionalization. The avirulent **XFL-7** strain (*i*) was obtained from 10403s strain of wt *Listeria monocytogenes* by knockout of the Positive Regulatory Factor A gene (*prfA*) (PMID: 11714814). PrfA is a transcription factor that regulates the expression of many virulent genes. Among them, Listeriolysin (LLO) is exploited by listeria to break free from cellular vacuoles and avoid digestion by lysosomes. The attenuated *Listeria monocytogenes* strain that we use, and that is widely employed as cancer vaccine, is in fact XFL-7 Lm^at-LLO strain (**Lm^at** for brevity, *ii*). Lm^at is obtained by transforming XFL-7 Lm^at strain with pGG-34-LLO plasmid. This plasmid drives the expression of PrfA, as well as that of a truncated version of Listeriolysin (LLO*), which can still mediate vacuole escape, but less efficiently compared to the wild type protein. The XFL-7 Lm^at-OVA strain (**Lm^at–OVA** for brevity, *iii*) is obtained by transforming XFL-7 strain with pGG-34-OVA plasmid, which expresses a fragment (aa 214-386) of chicken Ovalbumin instead of LLO*. This strain is avirulent, because unable to escape from vacuoles after host cell endocytosis (PMID: 30664692). Finally, **Lm^at-MAGEb** strain (*iv*), which is characterized by enhanced stimulation of the immune system against infected cancer cells, is obtained by transforming XFL-7 strain with pGG-34-LLO-MAGEb. This plasmid, together with LLO*, expresses a fragment (aa 311-660) of murine MageB Tumor Associated Antigen (PMID: 18728665).

(**b**) Cell wall functionalization of different Lm^at strains. The indicated strains of Lm^at were incubated ON with 40mM alkDA and then subjected to CuAAC reaction to obtain loading with AF488 green fluorophore. They all showed to be equally loaded, regardless of their genetic background. The graph represents the mean±SEM of at least three independent experiments. Unpaired t-test. ns: not significant.

Fig 1
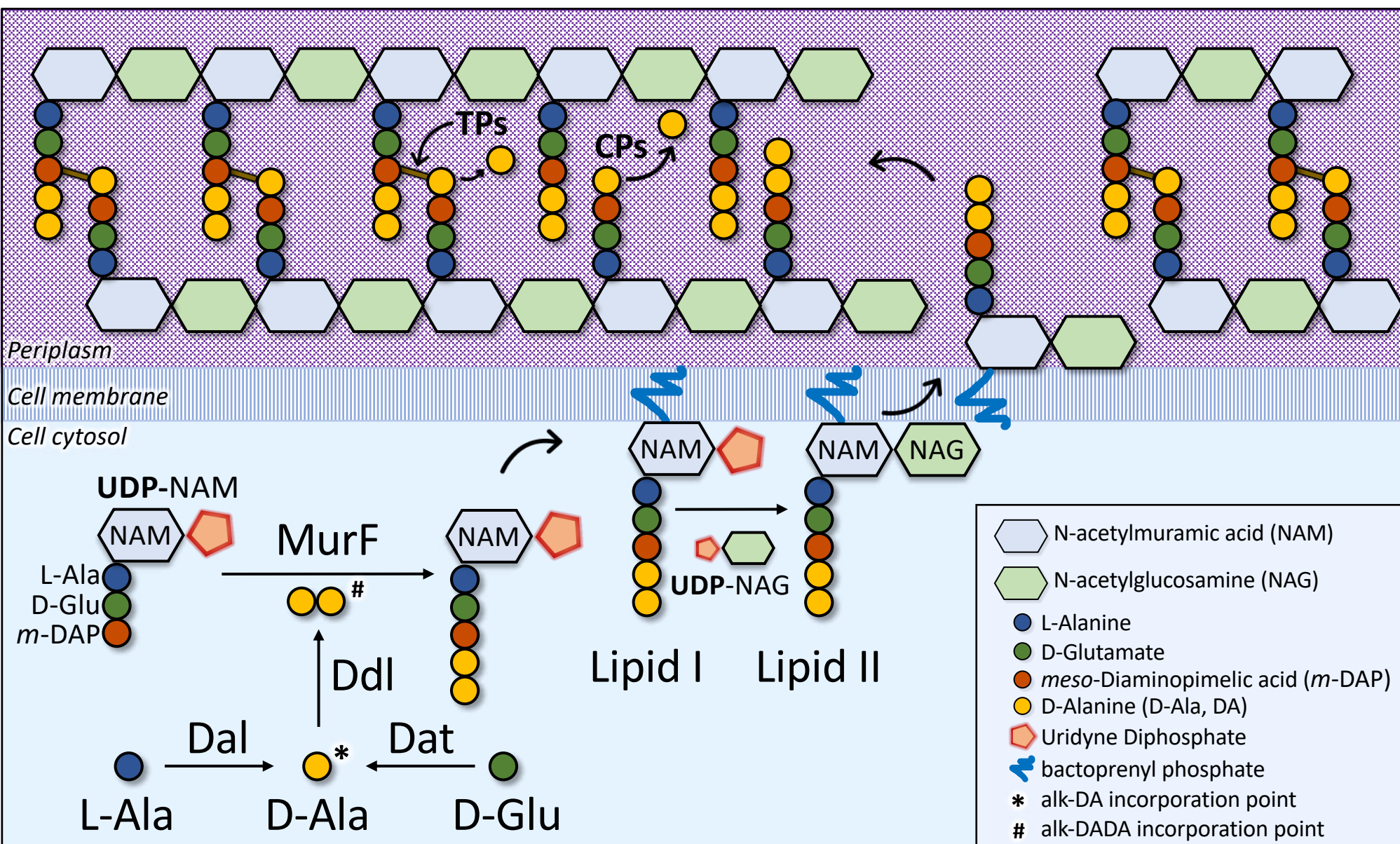
Supplementary Figure 6. Lm cell wall biosynthesis and points of alkDA and alkDADA probe incorporation.

The biosynthesis of Lm cell wall starts in the cytosol, where D-Alanine (D-Ala, DA) is generated from L-Alanine by D-Alanine racemase (Dal), or from D-Glutamate by D-amino acid aminotransferase (Dat). This is the main step where alkDA probe is incorporated. Then two D-Alanine are coupled by D-Alanyl-D-Alanine ligase (Ddl), to form D-Ala-D-Ala (DADA) dipeptide. This is the step where alkDADA probe is incorporated. Subsequently, UDP-N-acetylmuramoyl-tripeptide--D-alanyl-D-Alanine ligase (MurF) enzyme adds the DADA dipeptide to the pre-synthesized UDP-NAM-L-Ala-D-Glu-*m*-DAP unit, to generate the UDP-NAM-pentapeptide, which in turn is conjugated with bactoprenyl phosphate to generate Lipid I. At this point, UDP-NAG is added to Lipid I to generate Lipid II, which is flipped from the cytoplasmic to the periplasmic side of the cell membrane and employed to assemble the peptidoglycan (PG). Finally, remodelling enzymes cross-link the pentapeptide (a.k.a stem peptide) chains of one strand to the stem peptide chains of another strand, so that a 3D mesh-like layer is formed, which is strong and rigid. Specifically, D,D-carboxypeptidases (CPs, such as penicillin binding protein 5 (Pbp5)) remove the fifth D-Alanine of the stem peptide, while D,D-transpeptidases (TPs) remove the fifth D-Alanine of the stem peptide and cross-link the fourth D-Alanine to *meso*-Diaminopimelic acid.
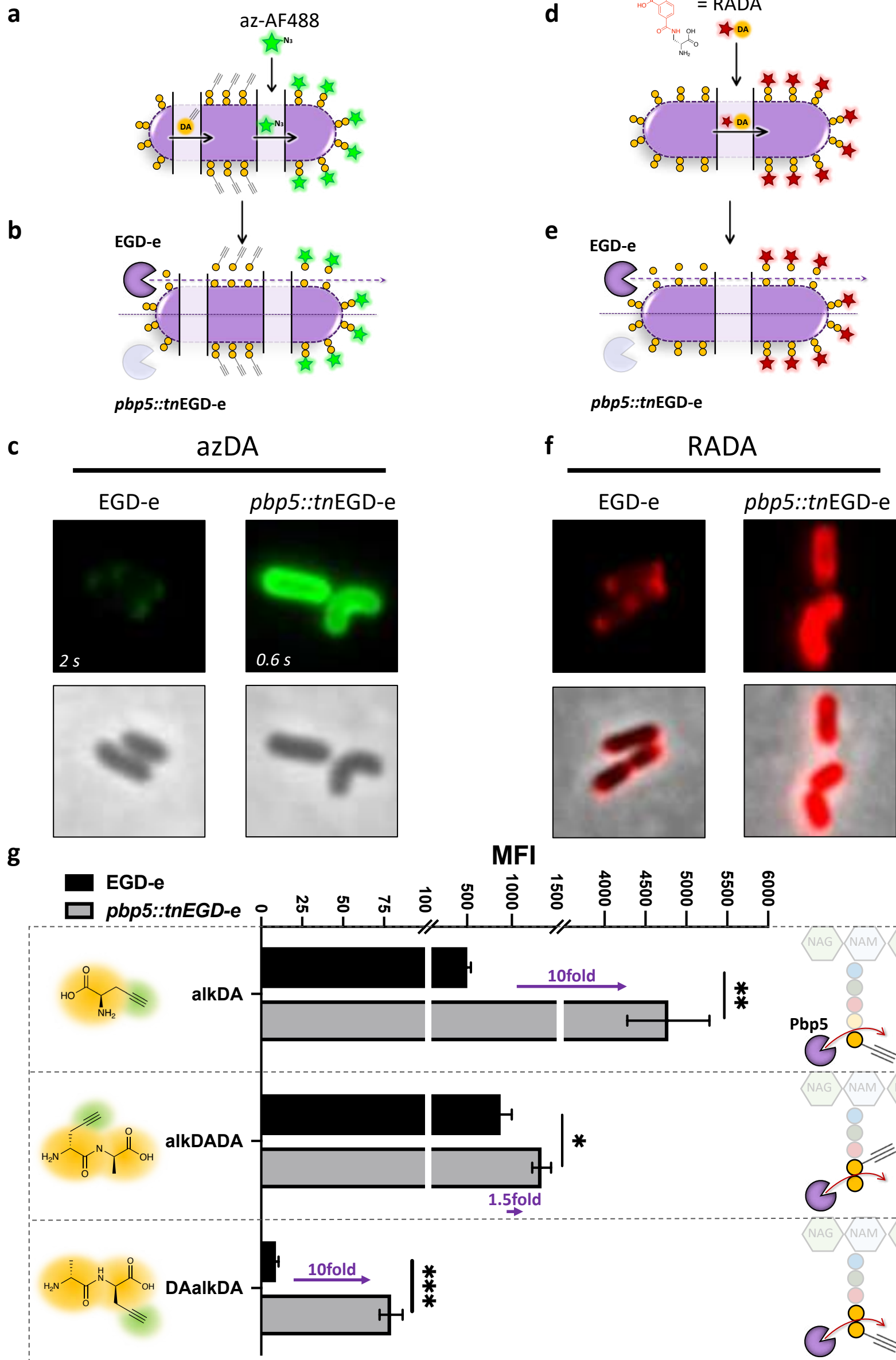
Supplementary Figure 7. Impact of the remodelling enzyme Pbp5 on *Listeria monocytogenes* cell wall functionalization.

(**a-c**) Impact of penicillin binding protein 5 (Pbp5) D,D-carboxypeptidase on the two-step loading approach using alkDA as probe. (**a**) Schematic representation of the two-step loading approach using alkDA as probe. (**b-c**) In the wt EGD-e Listeria strain (**b**, *upper*), Pbp5 removes the fifth D-Alanine of the stem peptide (yellow circle), resulting in decreased loading efficiency. Conversely, when the *pbp5::tn*EGD-e strain is used, which is deleted for Pbp5 (**b**, *lower*), the fifth D-Alanine is no longer removed and cell wall loading strongly increases. (**c**) Representative fluorescence microscope images of loaded EGD-e (*left*) and *pbp5::tn*EGD-e (*right*) strains. Images were taken at different exposure times (2sec for EGD-e and 0.6sec for *pbp5::tn*EGD-e) because of the strong difference in fluorescence intensity.

(**d-f**) Impact of Pbp5 enzyme on the one-step loading approach using RADA (rhodamine-D-Alanine) as probe. (**d**) Schematic representation of the one-step loading approach using RADA as probe. (**e-f**). The higher loading level of *pbp5::tn*EGD-e strain compared to wt EGD-e strain indicates that Pbp5 exerts a highly promiscuous activity and removes the fifth D-Alanine even when it carries bulky substituents on its side chain.

(**g**) Using alkDADA as probe, the impact of Pbp5 enzyme on the two-step loading approach is minimized. Metabolic labelling of wt EGD-e and *pbp5::tn*EGD-e Listeria strains was performed using alkDA (it incorporates in the fifth position of the stem peptide), alkDADA (it incorporates in the fourth and fifth position of the stem peptide and carries the alkyne group on the fourth D-Alanine), or DAalkDA (it incorporates in the fourth and fifth position of the stem peptide but carries the alkyne group on the fifth D-Alanine). Although basal incorporation varies from probe to probe and the cell wall of the mutant strain likely incorporates more probe because it is thicker (PMID: 16140473), the analysis of fluorescence intensity upon CuAAC reaction still indicates that Pbp5-mediated removal of the fifth D-Alanine is highly relevant only for alkDA and DAalkDA probes: the alk handle is expected to be incorporated on the fifth position of the stem peptide with both probes and, consistently, the MFI shown by the *pbp5::tn*EGD-e strain is much higher than that shown by the wt strain (~10fold). On the contrary, Pbp5-mediated removal of the fifth D-Alanine is much less impactful for alkDADA probe: the alk handle is expected to be incorporated on the fourth position of the stem peptide and, consistently, the MFI shown by the *pbp5::tn*EGD-e strain is just slightly higher than that shown by the wt strain (~1.5fold). The graph represents the mean±SEM of at least two independent experiments. Unpaired t-test. *p < 0.05, **p < 0.01, ***p < 0.001.
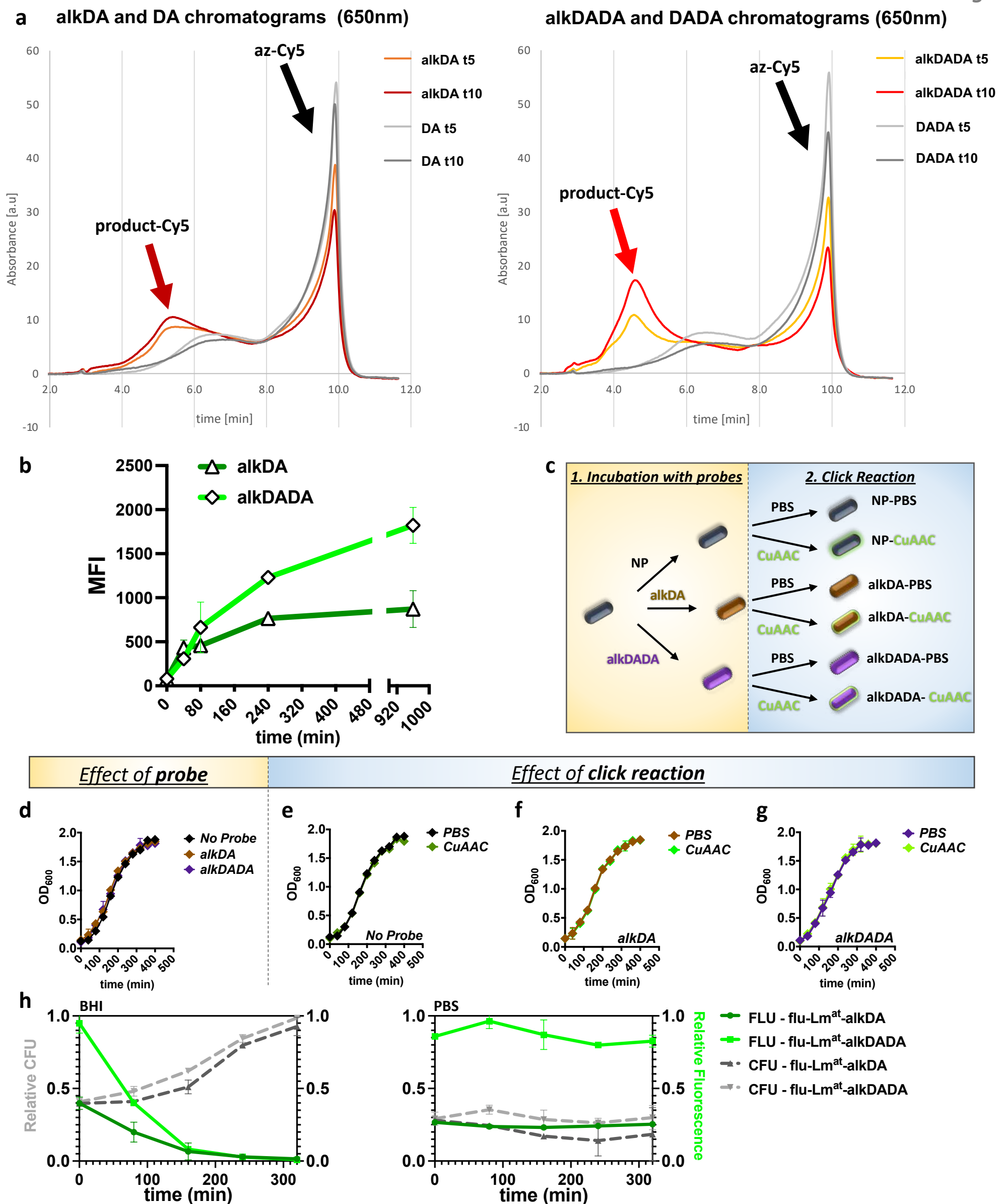
Fig 1

Supplementary Figure 8. Characterization of Lm^{at} functionalization with alkyne-D-Alanine (alkDA) and alkyne-D-Alanine-D-Alanine (alkDADA) probes.

(**a**) RP-HPLC analysis of the reactivity of alkDA probe (*left*) or alkDADA probe (*right*) with az-Cy5 fluorophore. A CuAAC reaction was set up in solution and the reaction mix was analyzed at different timepoints by reversed-phase (RP)-HPLC. Over time, a decrease in the size of az-Cy5 peak (black arrows) and a concomitant increase in the size of a peak with earlier elution time (red arrows) are observed, which is consistent with the reaction of the fluorophore with the probe. Probes with no alkyne group (DA and DADA, respectively) are used as negative controls (no peak with earlier elution time is observed).

(**b**) Fluorescence intensity of bacteria incubated with 40mM of alkDA or alkDADA probes for the indicated amount of time and then subjected to CuAAC reaction with az-AF488 fluorophore. Loading efficiency, determined by flow cytometry analysis in terms of median fluorescence intensity (MFI), is generally higher for alkDADA than alkDA. After ON incubation with the probes, a plateau is reached, which confirms that the maximal number of chemical handles have been incorporated on Lm^{at} surface.

(**c-g**) The optimized functionalization protocol does not affect Lm^{at} proliferation. (**c**) Schematic representation of the experimental set-up. In *Step 1*, Lm^{at} is incubated ON with 40nM alkDA or alkDADA. In *Step 2*, Lm^{at} from Step 1 is subjected to CuAAC reaction. (**d-g**) Proliferation of Lm^{at}, once subjected to the indicated experimental procedures. Refer to panel **c** for color coding.

(**h**) Loss of fluorescence by AF488-loaded Lm^{at}-alkDA and Lm^{at}-alkDADA over time. The loss of loading was investigated in two media: Brain Heart Infusion (BHI), which is the election growth medium for Lm^{at} (*left*), and the bacteriostatic PBS buffer (*right*). In BHI bacteria actively replicate (gray lines) and the loss of loading is fast (green lines). On the contrary, when bacteria are incubated in PBS, no proliferation is observed (gray lines), and, consequently, green fluorescence levels remain constant over time (green lines). These results suggest that replication is the main factor responsible for bacteria loss of loading over time. When alkDADA probe is used, fluorescence starts at higher level (see also **Figure 1b** and **panel b** above).

Graphs represent the mean±SEM of at least two independent experiments.

Fig 1
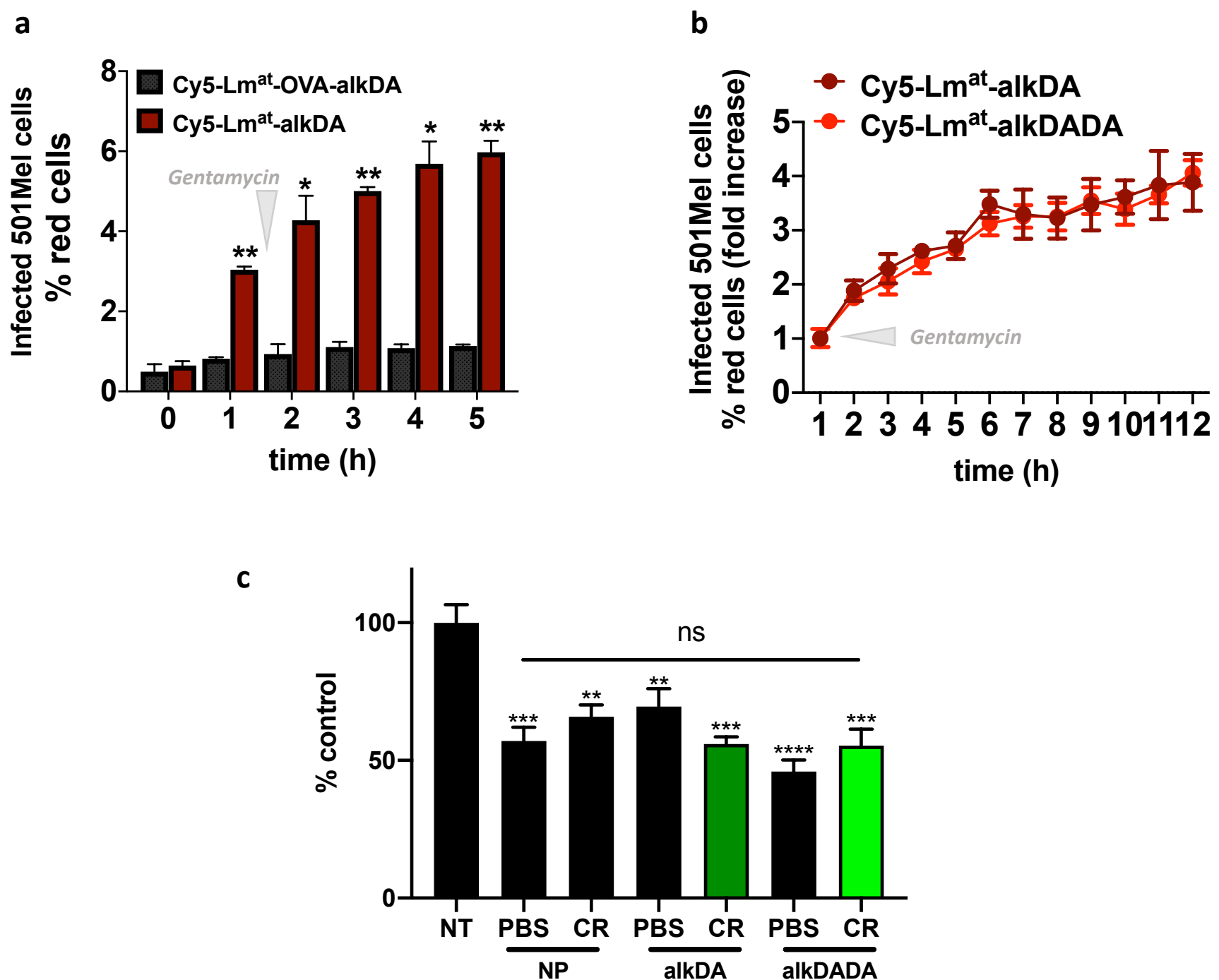
Supplementary Figure 9. Biological features of flu-Lm^{at}.

(**a-b**) Cell-to-cell spreading assay. As schematized in **Figure 1k**, 501Mel cells were infected at MOI 50. After 1h of infection, extracellular Lm^{at} was killed by medium replacement with fresh gentamycin-containing medium. Then, infected cells were collected at different time points post infection and directly analysed by flow cytometry to determine the percentage of cells that acquired red fluorescence due to listeria spreading. (**a**) Cell-to-cell spreading assay performed with Cy5-Lm^{at}-alkDA and Cy5-Lm^{at}-OVA-alkDA strains. Contrary to Cy5-Lm^{at}-OVA-alkDA strain, which is unable to spread because cannot escape from vacuoles after host cell endocytosis (grey bars), upon infection with Cy5-Lm^{at}-alkDA strain an increase in the percentage of red cells over time is detected (red bars). This result confirms that Lm^{at} spreading is the main reason why infected cells acquire red fluorescence, while the contribute of Lm^{at} turnover is minimal. (**b**) Cell-to-cell spreading assay performed with Cy5-Lm^{at}-alkDA and Cy5-Lm^{at}-alkDADA. Listeria shows similar spreading ability when metabolically labelled with both probes.

(**c**) Kill rate assay performed on A375 cells as reported in **Figure 1m** but using AF488-loaded Lm^{at} at MOI 200 instead of MOI 2000.

Graphs represent the mean±SEM of at least three independent experiments. Unpaired t-test. * $p < 0.05$, **$p < 0.01$, ***$p < 0.001$, ****$p < 0.0001$. ns: not significant.

Fig 2
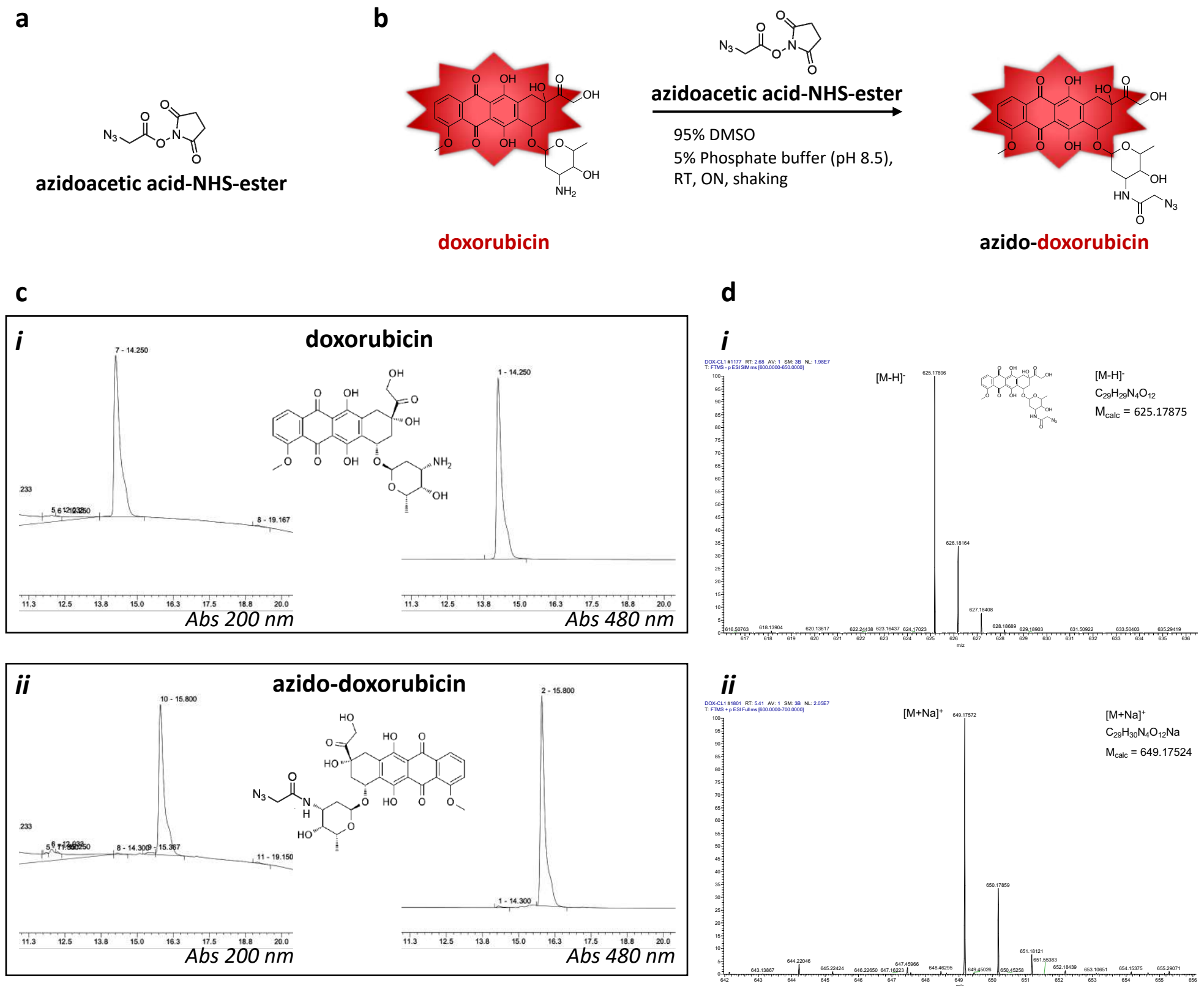
Supplementary Figure 10. Synthesis of azido-doxorubicin.

(**a**) Chemical structure of azidoacetic acid-N-hydroxysuccinimidyl (NHS)-ester.

(**b**) Schematic representation of the reaction conditions used to obtain azido-doxorubicin from doxorubicin and azidoacetic acid-N-hydroxysuccinimidyl (NHS)-ester.

(**c**) Chromatograms of doxorubicin (*i*) and azido-doxorubicin (*ii*), both at 200nm, to exclude the presence of non-fluorescent by-products (*left*), and at 480nm, the wavelength of maximum absorption of doxorubicin (*right*). Retention times: 14.250 minutes for doxorubicin and 15.800 minutes for azido-doxorubicin.

(**d**) High-Resolution Electron Spray Ionization mass spectrum of azido-doxorubicin in negative (*i*) and positive (*ii*) ion mode.

Fig 2
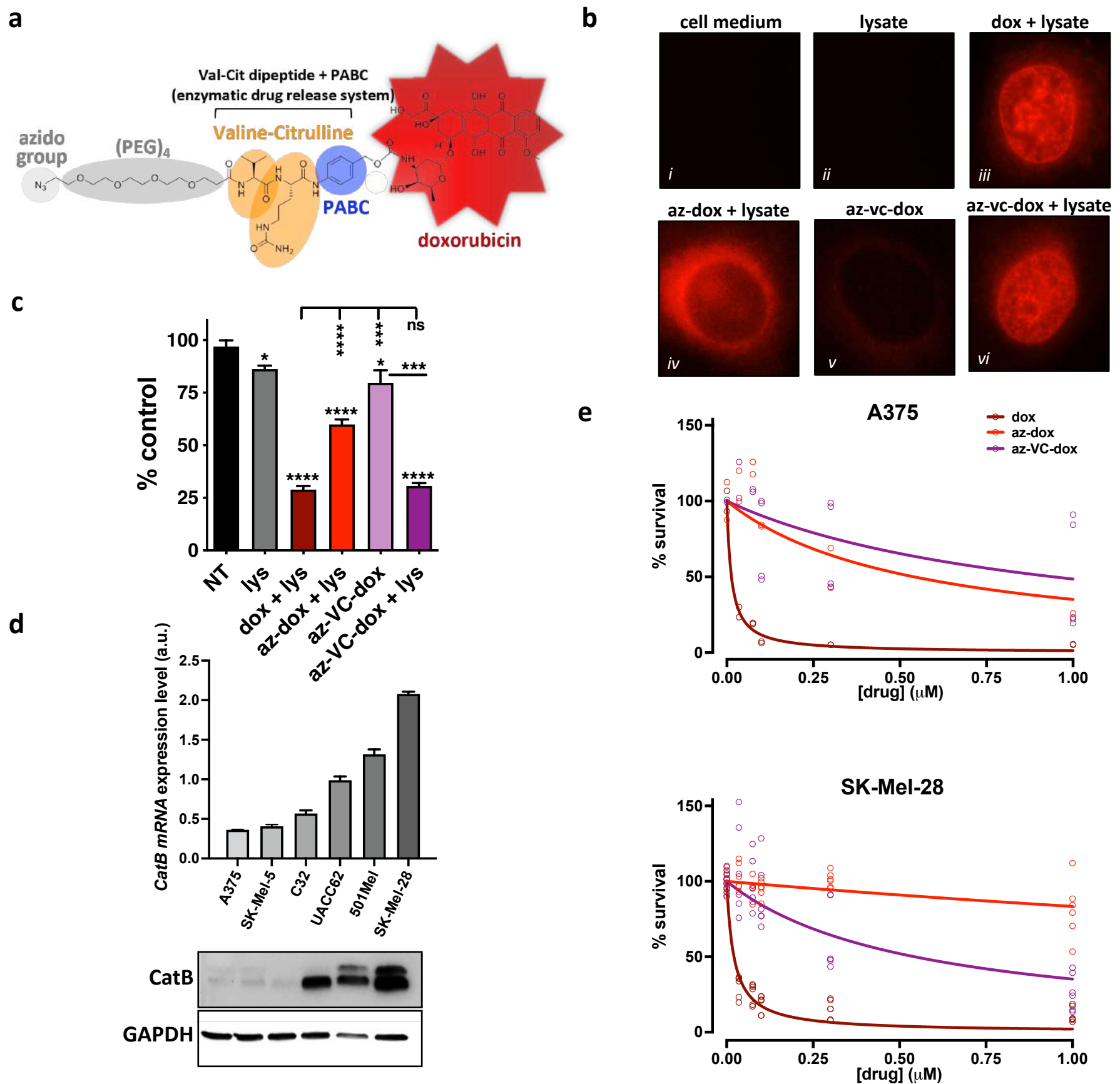
Supplementary Figure 11. Cathepsins-mediated cleavage of azido-Valine-Citrulline-doxorubicin and release of native drug in melanoma cell lines.

(**a**) Chemical structure of azide-PEG₄-Valine-Citrulline-PABC-doxorubicin (az-VC-dox). The compound contains: an azido group for click reaction with alkyne-labelled bacteria (light grey); a four units polyethylene glycol (PEG₄) spacer (grey) to increase molecule solubility; a Valine-Citrulline dipeptide (orange), which serves as drug release system in cancer tissues that overexpress Cathepsin enzymes; a *para*-aminobenzyl carbamate spacer (PABC, blue) directly attached to doxorubicin (red), *via* the amino group on the aminoglycoside portion of the drug. The PABC group acts as self-immolative spacer allowing the release of native doxorubicin after Cathepsin B cleavage of the Valine-Citrulline dipeptide.

(**b-c**) az-VC-dox cleavage by cellular Cathepsins restores fluorescence, nuclear localization, and cytotoxicity of doxorubicin. (**b**) Fluorescence microscope images of SK-Mel-28 melanoma cells incubated for 3h with: (*i*) cell medium; (*ii*) activated cell lysate from SK-Mel-28 cells; (*iii*) 3μM native dox in activated lysate; (*iv*) 3μM az-dox in activated lysate; (*v*) 3μM az-VC-dox in cell medium; (*vi*) 3μM az-VC-dox in activated lysate. Native doxorubicin can readily accumulate into cell nuclei. On the contrary, the drug loses this ability when functionalized on the primary amino group, both with small substituents like azidoacetic acid, and with the bulkier azido-Valine-Citrulline linker. The presence of the bulkier linker appears to quench red fluorescence as well. However, Cathepsins-mediated enzymatic cleavage of az-VC-dox fully restores doxorubicin fluorescence and nuclear localization, which is indicative of release in native form. Activation of Cathepsins present in cell lysate is induced by acidification up to pH4 (see Supplementary Methods for further details). If the lysate is kept at neutral pH, no cleavage of az-VC-dox is in fact observed (data not shown). The fluorescence and localization of native dox and az-dox in cell medium (data not shown) are indistinguishable from those displayed in activated lysate. (**c**) Kill rate assay performed on SK-Mel-28 cells treated for 48h with: cell medium (NT); activated cell lysate from SK-Mel-28 cells (lys); 0.3μM native dox in activated lysate (dox + lys); 0.3μM az-dox in activated lysate (az-dox + lys); 0.3μM az-VC-dox in cell medium (az-VC-dox); 0.3μM az-VC-dox in activated lysate (az-VC-dox + lys). Native doxorubicin is the most cytotoxic, while az-dox and especially az-VC-dox show reduced cytotoxicity. However, when az-VC-dox is incubated with the activated lysate, a full rescue in cytotoxicity is observed, which is consistent with the regain of nuclear localization (see panel **b**) and supports release in native form.

(**d-e**) Correlation between Cathepsin B levels and sensitivity to az-VC-dox. (**d**) Expression levels of Cathepsin B mRNA (qRT-PCR, *top*) and protein (western blot, *bottom*) in the indicated melanoma cell lines. (**e**) Survival curves of low Cathepsin B-expressing A375 melanoma cells (*top*) and high Cathepsin B-expressing SK-Mel-28 melanoma cells (*bottom*), treated with the indicated concentrations of doxorubicin (brown), az-dox (red) and az-VC-dox (purple) for 7 days. In the low Cathepsin B-expressing A375 melanoma cells, the cytotoxic effects of az-dox and az-VC-dox are very similar, while in the high Cathepsin B-expressing SK-Mel-28 melanoma cells az-VC-dox shows stronger cytotoxicity compared to az-dox, likely due to more efficient release of the native form of the drug through Cathepsin B-mediated cleavage.

Graphs represent the mean±SEM of at least three independent experiments. Unpaired t-test. *p < 0.05, ***p < 0.001, ****p < 0.0001. ns: not significant.
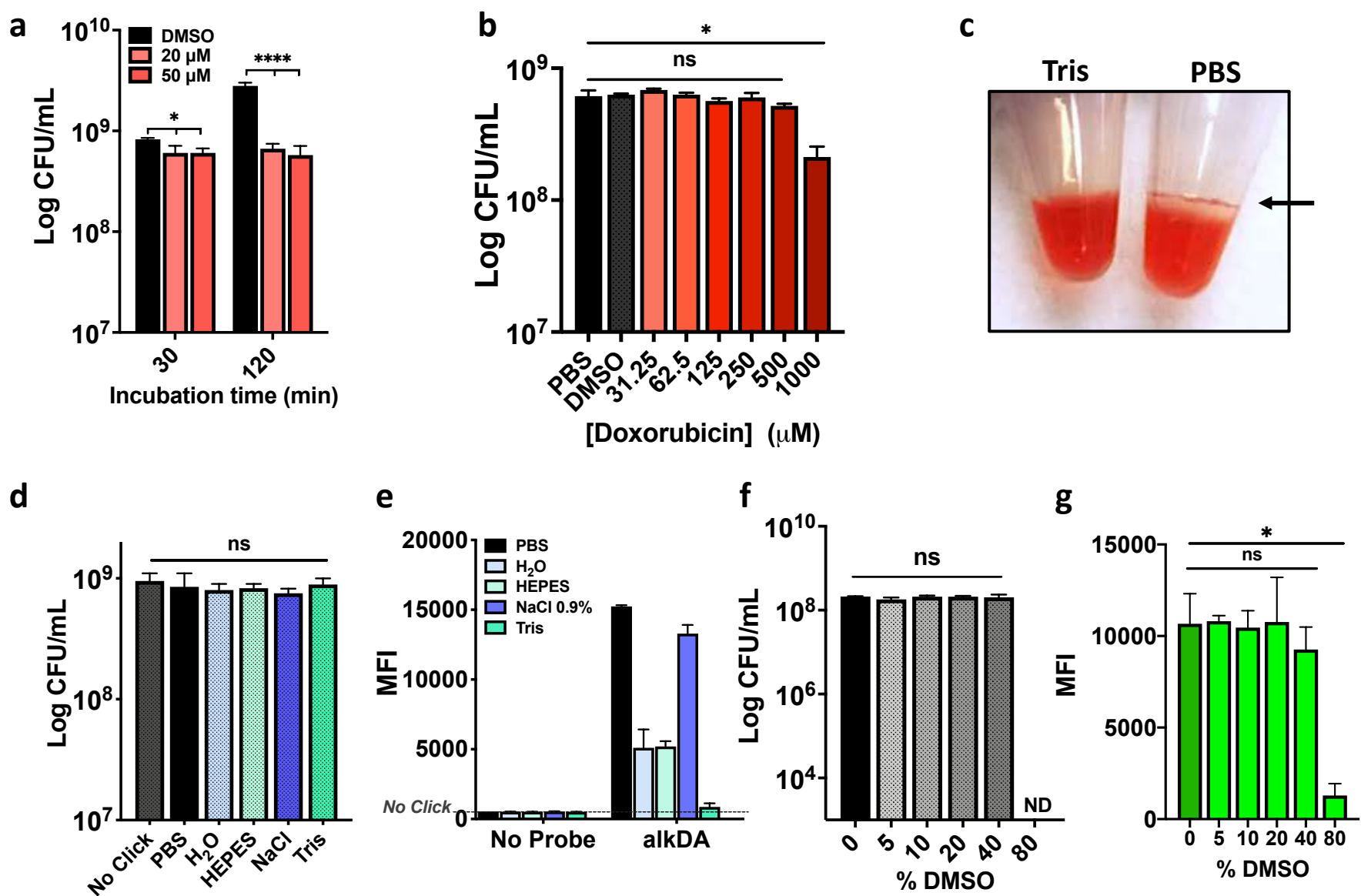
Fig 2

Supplementary Figure 12. Optimization of CuAAC reaction conditions for Lm[at] loading with az-dox and az-VC-dox.
(**a-b**) Evaluation of doxorubicin toxicity on Lm[at] in full medium (up to 120min, 37°C, BHI medium) (**a**), or in click reaction conditions (10min, room temperature, PBS buffer) (**b**). Doxorubicin is toxic for Lm[at] when incubated for a long time in BHI, which allows active replication. Conversely, when bacteria are kept for a short time in PBS, which is bacteriostatic, no toxic effect is observed even at very high dox concentrations (up to 500μM).
(**c**) Representative image of doxorubicin solubility/stability in Tris buffer (*left*) or PBS (*right*). The incubation of the drug in PBS (1mM, 2h, room temperature, shaking) leads to a cloudy suspension, with drug precipitates that are particularly evident on vial walls (arrow). Therefore, PBS cannot be used as buffer for CuAAC reaction.
(**d-g**) Viability and loading efficiency (measured as MFI) of Lm[at] incubated ON with 40mM alkDA probe and then subjected to CuAAC reaction, using az-AF488 as reaction partner and BTTP as ligand. Different solvents as alternatives to PBS and different concentrations of DMSO as co-solvent were tested. (**d-e**) When click reaction is performed in water, HEPES buffer, 0.9% w/v NaCl in water, or Tris buffer, Lm[at] viability is not affected (**d**). However, loading efficiency is comparable to that obtained with PBS only when 0.9% w/v NaCl in water is used (**e**). Tris buffer serves as negative control, as it is known to chelate copper ions and inhibit CuAAC (PMID: 22844652). (**f-g**) As co-solvent necessary for dox solubilization, DMSO does not affect Lm[at] viability (**f**) and loading efficiency (**g**), as long as its concentration is kept ≤40%.
MFI: median fluorescence intensity.
Graphs represent the mean±SEM of three independent experiments. Unpaired t-test. *p < 0.05, ****p < 0.0001. ns: not significant.

Fig 2

a

dox-Lm^{at} or dox-VC-Lm^{at}

incubate with **mutanolysin** and lysozyme

dox-Lm^{at} dox-VC-Lm^{at}

take the **supernatant** and quantify the amount of fluorescent drug by Tecan plate reader

b

β(1-4)glycosidic bond cleaved by mutanolysin/lysozyme

NAG   NAM

CH$_2$OH

OH

NH

H$_3$C—CO

CH—CH$_3$

CO

NH

COCH$_3$

pentapeptide

L-Ala
D-Glu
mDap
D-Ala
D-Ala (Gly)

c

pmol of dox loaded on 4x10^{8}CFU

900
700
500
300
200
100
10
0

** **
**

****

Lm^{at} dox-Lm^{at} dox-VC-Lm^{at}

d

% survival

150
100
50
0

pH 4
pH 8

ns   ns   ns   ns   *

lysate	+	+	+	+	+
dox (1µM)	-	+	-	+	-
Lm^{at} (4x10^8 CFU)	-	-	+	+	-
dox-VC-Lm^{at} (4x10^8 CFU)	-	-	-	-	+

Supplementary Figure 13. Characterization of dox loaded on dox-Lm^{at} and dox-VC-Lm^{at}.
(**a-c**) Quantification of loaded drug by extraction from bacterial cell wall. (**a**) Representative cartoon of the experimental protocol used to extract dox from Lm^{at} cell wall and to quantify it. The incubation of dox-Lm^{at} and dox-VC-Lm^{at} with a mix of mutanolysin and lysozyme enzymes allows to digest bacterial cell wall, and to recover intact cargos in the supernatant. Then, the amount of dox present in the supernatant is quantified by fluorescence measurement. Cartoon created with Biorender.com. (**b**) Mechanism of action of mutanolysin and lysozyme. These enzymes selectively cleave the NAM-NAG bond within the bacterial peptidoglycan (see also **Suppl. Fig. 6**), causing the break down of cell wall. (**c**) Picomols of dox loaded on 4x10^{8}CFU of dox-Lm^{at} (red) dox-VC-Lm^{at} (purple).
(**d**) Cathepsin-mediated release of dox from dox-VC-Lm^{at} cell wall. The release is measured as a statistically significant decrease in SK-Mel-28 cell survival, upon 48h treatment with medium obtained from the incubation of 4x10^8 CFU of dox-VC-Lm^{at} with the lysate of SK-Mel-28 cells, at pH8 (no activation of cellular Cathepsins, dark grey bar) vs pH4 (activation of cellular Cathepsins, light grey bar). Mock treatment with just the lysate is used as baseline. Treatment of SK-Mel-28 cells with lysate + 1µM dox is used as positive control of pH-insensitive decrease in cell survival. The decrease in cell survival observed by treatment of SK-Mel-28 cells with lysate + 4x10^8 CFU of unloaded Lm^{at} is likely attributable to the fact that Listeria secretes virulence factors (PMID: 30504226) and they persist in the medium used to treat SK-Mel-28 cells. In any case, the decrease does not depend on pH.
Graphs represent the mean±SEM of at least two independent experiments. Unpaired t-test. * p < 0.05, **p < 0.01, ****p < 0.0001. ns: not significant.

SUPPLEMENTARY METHODS

Reagents

Probes: alkyne-Dalanine (alkDA) (R-propargylglycine, Sigma-Aldrich or Acros Organics); 3-azido-D-alanine HCl ((R)-2-Amino-3-azidopropanoic acid hydrochloride, Jena Bioscience or Tocris Bioscience); EDA-DA and DA-EDA (custom made by WuXi AppTech); D-ala and D-ala-D-ala (Sigma-Aldrich). The pH of the aqueous probes solutions was checked before use and adjusted to 7 when necessary.

CuAAC reagents: $CuSO_4$ (Sigma-Aldrich); sodium ascorbate-L-(+) (Sigma-Aldrich); 3-(4-((bis((1-tert-butyl-1H-1,2,3-triazol-4-yl)methyl)amino)methyl)-1H-1,2,3-triazol-1-yl)propan-1-ol (BTTP) (Kumidas SA); BTTAA (Jena Bioscience).

Fluorophores: azide-AF488 (Jena Bioscience); alkyne-AF488 (Jena Bioscience); azide-Cy5 (Sigma-Aldrich); DBCO-AF488 (Jena Bioscience); azide-ATTO740 (ATTO-TEC GmbH).

Linkers: azidoacetic acid-N-hydroxysuccinimidyl (NHS) ester (Jena Bioscience); azide-PEG4-Valine-Citrulline-PABC-doxorubicin (Creative Biolabs).

Bacteria and cells growth media, supplements, and antibiotics: Brain Heart Infusion (BHI) (Sigma-Aldrich); Luria-Bertani (LB) (Sigma-Aldrich); Chloramphenicol (Sigma-Aldrich); DMEM High Glucose (HG), MEM and RPMI cell culture media (Euroclone); L-glutamine (Sigma-Aldrich); penicillin/streptomycin (Euroclone); gentamycin (Euroclone).

Drugs: doxorubicin hydrochloride (Sigma-Aldrich); SMER28 (Selleckchem).

Reagents for cell staining: paraformaldehyde (PFA) (Sigma-Aldrich); NOTOXhisto (Scientific Device Laboratory, Inc.); DAPI (4',6-Diamidino-2-Phenylindole, Dihydrochloride, Invitrogen); Fluoromount mounting glue (Bio-Optica).

alkyne-D-alanine-D-alanine, alkDADA

alkDADA (or EDA-DA) was synthesized as described in [1]. The recorded ^{1}H-NMR and ^{13}C-NMR spectra are in line with those reported in literature [1]. The purity of alkDADA was assessed by elementary analysis using Vario MICRO cube instrument (Elementar). Calculated for $C_8H_{12}N_2O_3 \cdot CF_3COOH$: C = 40.28; H = 4.39; N = 9.39. Experimental: C = 40.19; H = 4.68; N = 9.37.

Bacterial strains and culture conditions

Lm[at]-LLO [2], Lm[at]-OVA [2] and Lm[at]-MAGEb [3] strains were grown at 37°C in BHI medium with 34μg/mL chloramphenicol. EGD-e and *pbp5::tn*EGD-e strains [4] were grown at 37°C in BHI medium without antibiotics.

Cell culture

Melanoma cell lines were grown at 37°C in a humidified atmosphere containing 5 % CO_2. A375, 501 Mel, SK-Mel-28 and SK-Mel-5 cells were cultured in DMEM HG; C32 cells were cultured in MEM; UACC62 cells were cultured in RPMI. All media were supplemented with 10 % foetal bovine serum (FBS), 2 mM L-glutamine, 100 U/mL penicillin, and 100 μg/mL streptomycin or without antibiotics when infected with Lm[at].

Statistical analyses

Data were analyzed with unpaired t-test (*in vitro* assays) or Kruskal-Wallis test (Dunn's multiple comparisons test, xenograft assay), using GraphPad Prism, GraphPad Software Inc. Statistical significance was set at $p < 0.05$ (*$p < 0.05$, **$p < 0.01$, ***$p < 0.001$, ****$p < 0.0001$). The mean±SEM of at least three independent experiments is reported.

Methods used in Main Figures

Functionalization of Lm[at] with a fluorophore through metabolic labelling and CuAAC click reaction

A single colony of Lm[at] was inoculated in BHI +/- alkDA or alkDADA probes at 40 mM (or different concentrations when specified) and incubated overnight (ON, or shorter time points when specified) at 37°C in a shaking incubator. After OD_{600} normalization, metabolically labelled bacteria were washed three times in PBS to remove the excess of probe and

resuspended in PBS in half of the volume of CuAAC reaction mix: bacteria at 7.5×10^8 CFU/mL, 20 μM CuSO$_4$, 160 μM BTTP, 2.5 mM sodium ascorbate-L(+) (60 mM stock solution in water, freshly prepared), 25 μM azide-AF488 (or azide-Cy5 when specified). Chemical reagents were added one by one in this order and the solution was vortexed after each addition. After 10 min of incubation at room temperature in a shaking incubator, the reaction was stopped by adding an equal volume of 80 μM EDTA in PBS.

After click reaction, bacteria were washed three times in PBS, resuspended in PBS and analysed by flow cytometry (see below).

For stock preparation, bacteria where resuspended in DMEM HG, aliquoted, and stored at -80°C. The concentration of each stock was assessed by serial dilutions and plating for colony-forming units (CFU) on LB agar plates.

Functionalization of Lm^{at} with doxorubicin through metabolic labelling and CuAAC click reaction

A single colony of Lm^{at} was inoculated in BHI +/- 40 mM alkDADA and incubated ON at 37°C in a shaking incubator. After OD$_{600}$ normalization, metabolically labelled bacteria were washed three times in PBS to remove the excess of probe and resuspended in physiological solution (0.9% w/v NaCl in water) plus 25% DMSO in one third of the volume of CuAAC reaction mix: bacteria at 7.5×10^8 CFU/mL, 60 μM CuSO$_4$, 480 μM BTTP, 7.5 mM sodium ascorbate-L(+) (60 mM stock solution in water, freshly prepared), 200 μM azide-doxorubicin or azide-valine-citrulline-doxorubicin (or the control azide-ATTO 740, 5 μM). Chemical reagents were added one by one in this order and the solution was vortexed after each addition. After 7 min of incubation at room temperature in a shaking incubator, the reaction was stopped by adding an equal volume of 160 μM EDTA in physiological solution.

After click reaction, bacteria were washed four times in physiological solution plus 10% DMSO, resuspended in DMEM HG, incubated for 10 min at 37°C in a shaking incubator (to better remove doxorubicin derivatives non-covalently attached to bacteria surface), then centrifuged, resuspended in PBS, and analyzed by visual inspection, flow cytometry and fluorescence microscopy (see below).

For stock preparation, bacteria where resuspended in DMEM HG, aliquoted, and stored at -80°C. The concentration of each stock was assessed by serial dilutions and plating on LB agar plates.

Flow cytometry analysis of loaded Lm^{at}

10000 events were acquired using BD Accuri™ C6 (BD) and Mean Fluorescence Intensity (MFI) was used as measure of labelling efficiency. Data were analysed using FlowJo software.

Fluorescence microscopy of loaded Lm^{at}

Bacteria prepared on agar pad were imaged with Nikon Eclipse E600 or Zeiss Axioscope A1 with 100x objectives.

Fluorescence Lifetime Imaging (FLIM) of dox-Lm^{at}

dox-Lm^{at} was mounted on a slide using antifade glue, dried ON at 4°C, and imaged. FLIM experiments were performed by using a Leica TCS SP5 confocal microscope (Leica Microsystems). Doxorubicin was excited at 470 nm by a pulsed diode laser operating at 40 MHz and using a 100X, 1,3NA objective. Doxorubicin signal was collected through the same objective and filtered in the 520-650 nm range by a photomultiplier tube linked with a time correlated single photon counting card and setup (PicoHarp 300, PicoQuant). Phasor analysis of lifetime data was performed using SimFCS software (Laboratory for Fluorescence Dynamics, University of California, Irvine).

Viability of Lm^{at} after incubation with probes and/or CuAAC click reaction

A single colony of Lm^{at} was inoculated in BHI +/- alkDA or alkDADA probes at 40 mM (or different concentrations when specified) and incubated ON at 37°C in a shaking incubator. Viability was assessed by serial dilutions and plating for CFU on LB agar plates. The same approach was used to determine Lm^{at} viability at the end of the CuAAC reaction.

Proliferative activity of loaded Lm^at

Frozen aliquots of differently labeled Lm^{at} stocks were diluted in BHI to a starting concentration of 5×10^7 CFU/mL. Bacteria cultures were incubated in BHI at 37°C in a shaking incubator. Bacteria were collected at each time point and quantified by serial dilutions and plating for CFU on LB agar plates.

Infectivity and doubling time of loaded Lm^at

2.5×10^4 A375 cells were seeded in 24-well plates and after 16 h listeria at MOI 100 was added to the cells. After 1h (for fluorescent Lm^{at}) or 2h (for doxorubicin-loaded Lm^{at}), the medium was replaced with fresh medium containing 50 µg/mL gentamycin. At 3h and 6h post-infection (for fluorescent Lm^{at}) or at 3h and 18h post-infection (for doxorubicin-loaded Lm^{at}), A375 cells were washed once with PBS and then hot (approx. 60°C) sterile water was added to lysate them. After 10 min incubation at 37°C, the concentration of intracellular bacteria was assessed by dilution and plating for CFU on LB agar plates.

In the case of SMER28 treatment, the infectivity protocol described above was modified as follows. 3.5×10^4 A375 cells were seeded in 24-well plates and after 8h they were treated with or 50 or 200 µM SMER28 for 16h. The day after, listeria at MOI 100 was added to the cells. After 2h the medium was replaced with fresh medium containing 50 µg/mL gentamycin. At 3h post-infection, A375 cells were washed once with PBS and then processed as mentioned above.

Bacterial doubling time was calculated as the ratio of CFU at 6h vs 3h, using the Roth V. 2006 Doubling Time Computing Tool (http://www.doubling-time.com/compute.php).

Immunofluorescence of cells infected with loaded Lm^at

flu-Lm^at-alkDA and flu-Lm^at-alkDADA

10^4 A375 cells were seeded in 24-well plates containing round coverslips and after 16h Lm^{at} at MOI 100 was added to the cells. After 1h, the medium was replaced with fresh medium containing 50 µg/mL gentamycin and cells were incubated for 2 additional hours. Then, cells were washed two times with PBS and fixed in PFA (4% in PBS) for 15 min at room temperature. After 3 washes in PBS, cells were incubated with blocking solution (1% BSA, 0.1% Triton X-100 in PBS) for 15 min at room temperature. Then, the solution was replaced with blocking solution containing a 1:5000 dilution of the primary anti-listeria antibody (Listeria O antiserum poly serotypes 1 and 4, #223021, BD) for 90 min at room temperature. After three 5-min washes with PBS, Alexa Fluor™ 647 Goat anti-Rabbit IgG (H+L) Highly Cross-Adsorbed Secondary Antibody secondary antibody (#A-21245, Thermo Fisher Scientific) was diluted 1:250 in blocking solution and was incubated for 1h at room temperature in the dark. The blocking solution of the secondary antibody also contained 300nM DAPI for nuclei staining in blue and 1:1000 Alexa Fluor™ 594 Phalloidin (#A12381, Thermo Fisher Scientific) for staining of actin filaments in red. After three 5-min washes with PBS, glasses were mounted on microscope slides using antifade glue (BioOptica) and let dry ON at 4°C.

Slides were visualized on a Leica SP2 confocal microscope equipped with an AOBS system using a 63Å~ oil immersion objective. Images were subsequently analyzed using ImageJ software. Regardless of staining with anti-Listeria antibody, the green channel was used for a direct visualization of Lm^{at} loaded with AF488 fluorophore.

dox-Lm^at

Compared to the protocol described above, actin filaments were stained in green using 1:1000 Alexa Fluor™ 488 Phalloidin (#A-12379, Thermo Fisher Scientific), while dox-Lm^{at} was visualized directly using the red channel.

Cell-to-cell spreading of fluorescent Lm^at (*protocol with anti-Listeria antibody*)

2.5×10^5 501 Mel cells were seeded in 6-well plates in complete DMEM HG w/o antibiotics. After 24h, cells were infected with MOI 50 of Lm^{at} that was previously labelled with alkDA or alkDADA probe and subjected to CuAAC click reaction with 25 µM azide-Cy5 fluorophore. After 2h of infection, the extracellular Lm^{at} was killed by replacing the medium with fresh DMEM HG medium containing 50 µg/mL gentamycin. At 3h and 18h post infection cells were washed with PBS, collected, and incubated with blocking solution (1% BSA, 0.001% Nonidet in PBS) containing 1:250 primary anti-Listeria antibody (Listeria O antiserum poly serotypes

1 and 4, #223021, BD) for 6h at 4°C. Cells were then washed twice in PBS and incubated in blocking solution with a 1:500 dilution of secondary antibody (Alexa Fluor™ 488 Goat anti-Rabbit IgG (H+L) Highly Cross-Adsorbed Secondary Antibody, #A-11034, Thermo Fisher Scientific) for 40 min at room temperature. Finally, cells were washed twice with PBS and the percentage of infected green cells was analysed by flow cytometry (CytoFLEX V2-B2-R0 Flow Cytometer (4 Detectors, 2 Lasers) B53017, Beckman Coulter). Data analysis was performed by FlowJo.

Kill rate of loaded Lm^{at}
10^3 A375 cells were seeded in 96-well plates in complete DMEM HG w/o antibiotics. After 16h cells were infected with MOI 2000 (or different MOI when specified) of Lm^{at} and after 3h the medium was replaced with fresh medium containing 50 μg/mL gentamycin. After 24h (for fluorescent Lm^{at}) or 48h (for doxorubicin-loaded Lm^{at}), cells were fixed with NOTOXhisto, according to the manufacturer's protocol, and stained with 300nM DAPI. Cells nuclei where then counted by fluorescent microscopy. 3 fields per well were visualized with Nikon EclipseTi2 fluorescent microscope equipped with a Nikon camera (Nikon NIS Elements software), 20x objective.

Immunofluorescence staining of MCM7 proliferation marker upon infection with doxorubicin-loaded Lm^{at}
$7x10^3$ A375 melanoma cells were seeded in 24-well plates containing round coverslips and 24 h later they were infected with dox-Lm^{at}, dox-VC-Lm^{at} or flu-Lm^{at} at MOI 1000. After 3h of infection, the medium was replaced with fresh medium containing 50 μg/mL gentamycin, and cells were incubated for additional 48 hours. Cells were then washed two times in PBS and fixed with 4% PFA in PBS for 10 min at room temperature. After 3 washes in PBS, cells were permeabilized by incubation with 0.5% Triton-X-100 in PBS for 10 min at room temperature. Cells were then washed three times in PBS and incubated in blocking solution (1% BSA in PBS) for 30 min at room temperature. Cells were then stained with a 1:50 dilution of anti-MCM7 mouse monoclonal primary antibody (clone 141.2, #sc-9966, Santa Cruz Biotechnology) in blocking solution ON at 4°C. After three washes with PBS, cells were incubated with a 1:500 dilution of the secondary antibody (Alexa Fluor™ 488 Goat anti-Mouse IgG (H+L) Highly Cross-Adsorbed Secondary Antibody, #A-11029, Thermo Fisher Scientific) in blocking solution in the dark for 30 min at room temperature. The blocking solution of the secondary antibody contained 300nM DAPI for nuclei staining in blue. Following three washes with PBS, the coverslips were mounted on a microscope slide by using Fluoromount mounting glue and let dry ON at 4°C.
Slides were visualized with Nikon EclipseTi2 fluorescent microscope equipped with a Nikon camera (Nikon NIS Elements software), 60x oil objective.

Zebrafish husbandry
The Zebrafish facility at CNR-IFC has been authorized by the Italian Ministry of Health (authorization #297/2012-A, issued on December 21, 2012) and by the Municipality of Pisa (authorization #DN-16/504, issued on June 7, 2013). Zebrafish (*Danio rerio*) experiments were carried out in accordance with the European Union guidelines for animal welfare [European Communities Council Directive of September 22, 2010 (2010/63/UE)]. All experimental protocols were approved by the Italian Ministry of Health (authorization #383/2020-PR).
Zebrafish are raised and maintained on a 14h/10h light/dark cycle at 28.5°C, in a zebrafish housing system (Tecniplast) under pH- and salinity-controlled conditions. Embryos are obtained by natural spawning, are maintained in E3 medium (5mM NaCl, 0.17mM KCl, 0.33mM CaCl2, 0.33mM MgSO4), and are staged according to hours post fertilization (hpf) and morphologic criteria [5]. Embryos euthanasia is performed by hypothermia shock for at least 20min, while adults are euthanized by exposure to excess of tricaine methanesulfonate (MS-222, #A5040, Merck).

Xenograft in zebrafish embryos
$1x10^6$ A375-PIG cells, which are stably infected with PIG-NotI (PIG) plasmid, hence stably express eGFP [6], were seeded in 100mm plates (1 plate per experimental condition) in complete

DMEM HG w/o antibiotics. After 24h, cells were infected with flu-Lm[at] or dox-Lm[at] at MOI 1000. After 2h, medium was replaced with fresh medium containing 50 μg/mL gentamicin. After an additional hour, infected cells were harvested using trypsin, counted, centrifuged and washed once with PBS. Then PBS was completely removed, and the tube was cooled down on ice. Cells were carefully resuspended in matrigel (Corning® Matrigel® Growth Factor Reduced (GFR) Basement Membrane Matrix, #354230) to reach the final concentration of 250 cells/nl (4ul of matrigel per 1x10^{6} cells), by using cold pipette tips and avoiding bubble formation [7].

In the meantime, germ-free embryos of the *casper* line (ZDB-GENO-080326-11 line, kindly provided by Dr. Santoro, University of Padua, Italy) were generated as described in [8]. In brief, eggs were collected immediately after spawning and transferred to a sterile dish with sterilised E3 medium containing antibiotics (100 μg/mL ampicillin, 50 μg/mL gentamicin, 5 μg/mL kanamycin and 5 μg/mL amphotericin B). Embryos were monitored every 2h and unfertilized eggs were removed.

At 48hpf, embryos were manually dechorionated with forceps (Dumont No.5, #F6521-1EA, Sigma-Aldrich) and anaesthetised with 0.17 mg/mL tricaine (Sigma-Aldrich, #A5040). Cell suspension was loaded into a borosilicate glass capillary and 1nl (0,15mm, 250 cells) was injected into the yolk sac of the dechorionated embryos, using a microinjector (Tritech Research). After injection, embryos were allowed to grow in E3 medium for 48h at 34°C. In order to limit mortality caused by high bacterial load in the medium, embryos were washed twice a day with E3 medium supplemented with 50 μg/mL gentamicin. At least 100 embryos were injected per experimental condition.

Pictures of xenografts were acquired at 3 and 48h post-microinjection. Fluorescence imaging was carried out using Leica MZ10F stereomicroscope equipped with DFC3000 G camera and LAS X software version 3.7.0.20979. Area of cancer cell mass was measured using ImageJ software (http://rsb.info.nih.gov).

Xenograft experiments were performed in A375 cells for consistency with kill rate assays (**Fig. 1m and 2j**) and because we have extensively used them for this purpose [6] [9] [7]. In addition, xenograft experiments were performed only with dox-Lm[at] for the following reasons. Kill rate assay indicates that dox-Lm[at] and dox-VC-Lm[at] have similar efficacy. Therefore, in compliance with the 3R principles, we opted for testing only one of the two types of dox-loaded *Listeria*. dox-Lm[at] was chosen over dox-VC-Lm[at] because it is less expensive (it does not contain the azide-PEG4-Valine-Citrulline-PABC-doxorubicin linker, which is a custom synthesis that we purchase from Creative Biolabs).

Comparison between SPAAC and CuAAC click reactions

A single colony of Lm^{at} was inoculated in BHI +/- azDA probe at 2.5 mM (or different concentrations when specified) and incubated ON at 37°C in a shaking incubator. After OD$_{600}$ normalization, metabolically labelled bacteria were washed three times in PBS to remove the excess of probe and resuspended in PBS in half of the volume of SPAAC reaction mix or CuAAC reaction mix. SPAAC reaction mix: bacteria at 7.5x10^8 CFU/mL, 25 μM DBCO-AF488 in PBS. CuAAC reaction mix: bacteria at 7.5x10^8 CFU/mL, 200 μM CuSO$_4$, 800 μM BTTP (or BTTAA when specified), 2.5 mM (or other concentrations when specified) sodium ascorbate-L(+) (60 mM stock solution freshly prepared in water), 25 μM alkyne-AF488. Chemical reagents were added one by one in this order and the solution was vortexed after each addition. The reaction was incubated for 30 min (or different time when specified) at room temperature in a shaking incubator, then it was stopped by adding an equal volume of 80 μM EDTA in PBS.

After click reaction, bacteria were washed three times in PBS, resuspended in PBS and analysed by flow cytometry (10000 events, C6 Accuri™, BD).

Functionalization of wildtype EGD-e Lm and *pbp5::tn*EGD-e strains with a fluorophore through metabolic labelling and CuAAC click reaction

A single colony of wildtype EGD-e Lm or *pbp5::tn*EGD-e Lm was inoculated in BHI with alkDA, alkDADA or DAalkDA probes at 1 mM and incubated overnight (ON) at 37°C in a shaking incubator. After OD$_{600}$ normalization, metabolically labelled bacteria were washed three times in PBS to remove the excess of probe and resuspended in half of the volume of CuAAC reaction mix: bacteria at 7.5x10^8 CFU/mL, 20 μM CuSO$_4$, 160 μM BTTP, 2.5 mM sodium ascorbate-L(+) (60 mM stock solution in water, freshly prepared), 50 μM CalFluor 580 Azide (Vector Laboratories, #CCT-1371). Chemical reagents were added one by one in this order and the solution was vortexed after each addition. After 30-60 min at room temperature in a shaking incubator, the reaction was stopped by adding an equal volume of 80 μM EDTA in PBS.

After click reaction, bacteria were washed three times in PBS, resuspended in PBS and analysed by flow cytometry.

Functionalization of wildtype EGD-e Lm and *pbp5::tn*EGD-e strains with RADA probe

Wildtype EGD-e Lm and *pbp5::tn*EGD-e strains were incubated with 0.25 mM RADA at 37°C ON in BHI. The day after the culture was collected, washed three times with PBS and observed by fluorescence microscopy.

Reactivity of az-Cy5 with alkDA and alkDADA

To test the reactivity of az-Cy5 with alkDA and alkDADA, a click experiment was set up in solution and the reaction mix was analyzed at different timepoints by reversed-phase (RP)-HPLC. The CuAAC reaction mix was composed of: 100 μM alkDA/alkDADA, 25 μM azido-Cy5, 2,5 mM NaAsc, 20 μM CuSO4, 160 μM BTTP in PBS. In alternative, 100 μM DA/DADA probes (no alk handle) were used as negative controls. After 5-20 min at room temperature in a shaking incubator, the reaction was stopped by adding Sodium EDTA to 100μM. Reaction products were immediately subjected to a RP-HPLC run, using the following experimental conditions: Column LunaC8 Phenomenex; Mobil Phase Water/ACN 0,1% TFA; gradient from 0% to 100% ACN in 20' starting from min 3; 20 μL injection.

Loss of fluorescence of Lm^{at} over time

Frozen aliquots of flu-Lm^{at}-alkDA and flu-Lm^{at}-alkDADA stocks were centrifuged and resuspended in BHI or PBS to obtain a concentration of 5x10^6 CFU/mL. Bacteria suspensions were incubated for 320 min at 37°C in a shaking incubator. Every two doubling (80 min), aliquots of bacteria were collected, serially diluted, then plated for CFU on LB agar plates or analyzed by flow cytometry.

Cell-to-cell spreading assay of fluorescent Lm^{at} (*protocol without anti-Listeria antibody*)

3x10^4 of 501 Mel cells were seeded in 96-well plates in DMEM HG + 10% FBS w/o antibiotics. After 16h, cells were infected with MOI 50 of Lm^{at} previously labelled with alkDA or alkDADA

probe and subjected to CuAAC click reaction with 25 μM azide-Cy5 fluorophore. After 1h of infection, the extracellular Lm^{at} was killed by replacing the medium with fresh DMEM medium containing 50 μg/mL gentamycin. At different time points cells were washed twice with PBS and collected. The percentage of infected red cells was analysed by flow cytometry (10000 events, BD Accuri™ C6, BD). Data analysis was performed by FlowJo.

Synthesis and analysis of azido-doxorubicin
Doxorubicin hydrochloride (Sigma-Aldrich) powder was resuspended in DMSO at a concentration of 1 mg/mL. Azidoacetic acid-N-hydroxysuccinimidyl (NHS) ester was resuspended with anhydrous DMSO in anhydrous atmosphere, aliquoted, and stored at -20°C. Reaction conditions: 2.6 mM doxorubicin, 52.5 mM azidoacetic acid-NHS ester in 95% DMSO and 5% phosphate buffer (50 mM, pH 8.5). The reaction was incubated for 16h at room temperature in a shaking incubator.

Purification and analysis were performed with reverse phase HPLC chromatography (Ultra-high-performance liquid chromatograph UltiMate® 3000, Dionex) on C18 column (Luna® 5 μm C8(2) 100 Å, LC Column 250 x 4.6 mm, Ea, part number 00G-4249-E0). Elution was performed at 1 mL/min. A 20 min linear gradient of acetonitrile, ranging from 25 to 75% in 0,1% trifluoroacetic acid (TFA) in water, was used. Wavelenghts: 200 nm, to exclude the presence of non-fluorescent by-products; 480 nm, which is the wavelength of maximum absorption of doxorubicin. Retention times: 14.250 min for doxorubicin; 15.800 min for azido-doxorubicin.

Azido-doxorubicin was also analyzed in negative and positive ion mode by High-Resolution Electron Spray Ionization mass spectrometry, using a Thermo LTQ Orbitrap XL mass spectrometer (Thermo Fisher Scientific).

Doxorubicin toxicity towards Lm^{at}
Doxorubicin toxicity on Lm^{at} was assessed both in proliferative and bacteriostatic conditions, the latter mimicking CuAAC reaction conditions.

To investigate doxorubicin toxicity in proliferative conditions, a single colony of Lm^{at} was inoculated in BHI and incubated ON at 37° C in a shaking incubator. The day after bacteria culture was diluted 1:3 in BHI containing 20 or 50 μM doxorubicin and incubated at 37°C in a shaking incubator. After 30 or 120 min Lm^{at} viability was assessed by serial dilutions and plating for CFU on LB plates.

To investigate doxorubicin toxicity in bacteriostatic conditions, after an overnight growth, bacteria culture was centrifuged and resuspended in PBS containing different concentrations of doxorubicin. After 10 min of incubation at room temperature in a shaking incubator, Lm^{at} viability was assessed by bacteria dilutions and plating for CFU on LB plates.

CuAAC click reaction in different solvents
A single colony of Lm^{at} was inoculated in BHI with 40 mM alkDA and incubated ON at 37°C in a shaking incubator. After OD$_{600}$ normalization, metabolically labelled bacteria were washed three times in PBS to remove the excess of probe and resuspended in half of the volume of CuAAC reaction mix (10 μM CuSO$_4$, 80 μM BTTP, 1.25 mM freshly prepared sodium ascorbate-L(+), 25 μM azide-AF488) in different solvents: PBS, 20 mM Tris-HCl, 100 mM HEPES, physiological solution (0.9% w/v NaCl in water), water. Chemical reagents were added one by one in this order and the solution was vortexed after each addition. After 10 min of incubation at room temperature in a shaking incubator, the reaction was stopped by adding an equal volume of 160 μM EDTA. To determine loading efficiency, bacteria were washed three times in PBS, resuspended in PBS, and analysed by flow cytometry (10000 events, C6 Accuri™, BD). Bacteria viability was assessed by serial dilutions and plating for CFU on LB plates.

CuAAC click reaction at increasing concentrations of DMSO as co-solvent
A single colony of Lm^{at} was inoculated in BHI with 40 mM alkDA and incubated ON at 37°C in a shaking incubator. After OD$_{600}$ normalization, metabolically labelled bacteria were washed three times in PBS to remove the excess of probe and resuspended in half of the volume of CuAAC reaction mix (10 μM CuSO$_4$, 80 μM BTTP, 1.25 mM fresh prepared sodium

ascorbate-L(+), 25 μM azide-AF488) containing increasing percentages of DMSO. Chemical reagents were added one by one in this order and the solution was vortexed after each addition. After 10 min of incubation at room temperature in a shaking incubator, , the reaction was stopped by adding an equal volume of 160 μM EDTA. To determine loading efficiency, bacteria were washed three times in PBS, resuspended in PBS, and analysed by flow cytometry (10000 events, C6 Accuri™, BD). Bacteria viability was assessed by serial dilutions and plating for CFU on LB plates.

Cleavage of azido-VC-dox using SK-Mel-28 cell lysate
Two 75 mL flasks were seeded with 2×10^6 SK-Mel-28 cells each. After 48h, cells were collected by trypsinization and counted. 8×10^6 cells were washed twice in 25 mL PBS and then centrifuged. The pellet was lysed in 3 mL of water, vortexed, and incubated for 15 min at 4°C in a shaking incubator. Then, to favor protein solubilization, 1.5 mL of acetone was added to the mixture and incubated for additional 15 min under the same conditions. To remove cell debris, the suspension was centrifuged at 7000 rcf for 10 min at 4°C. The supernatant was collected and concentrated in Speedvac to completely remove the acetone. Then, to activate cytoplasmic Cathepsins, the lysate was acidified by adding 0,2M HCl up to pH 4. The acidic lysate containing active Cathepsins was used to cleave 9μM az-VC-dox linker (3x concentration) by ON incubation at 37°C. The mixture was centrifuged to remove precipitated cell debris, then two volumes of complete DMEM medium were added to one volume of supernatant and the pH was adjusted to 8, adding 0,2 M NaOH if needed. Activated lysate was added to A375 cells seeded the day before on glass-bottom plates (CELLview™ Cell Culture Dish, four compartments, Thermo Fisher Scientific) at the density of 10^4 cells per compartment. Cells were imaged after 3h of incubation, using Nikon EclipseTi2 fluorescent microscope equipped with a Nikon camera (Nikon NIS Elements software), 60x oil objective.

mRNA expression levels of cathepsin B through qRT-PCR
Total RNA was extracted using QIAzol reagent (Qiagen), following the manufacturer's instructions. RNA was quantified using Nanodrop Lite (Thermo Fisher Scientific). 1 μg of RNA was retrotranscribed using QuantiTect Reverse Transcription Kit (Qiagen), following the manufacturer's instructions and using a S1000 Thermal Cycler (Bio-Rad). Genomic contamination of RNA was ruled out by PCR on the cDNA using PCR Master Mix (Thermo Fisher Scientific) and *ATPA1* primers [10].
Quantitative PCR was performed using SsoAdvanced Universal Supermix (Bio-Rad) on a CFX96 Real-Time System (Bio-Rad).
The reaction conditions were the following: 98 °C 30 s, (98 °C 3 s, 58 °C 20 s, 72 °C 10 s) ×40 cycles. In order to confirm the specificity of the reaction, a melting curve was performed after each PCR (from 65 °C to 95 °C with an increase of temperature of 0.5 °C/s). Reactions were performed in duplicate, and the average of the two Ct values was used to calculate the expression of the different transcripts by the $2^{-\Delta\Delta Ct}$ method, using the geometrical square mean of three housekeeping genes (*GAPDH*, *PBG*D, *SDHA*) as a reference [6].
PCR and qRT-PCR primers were purchased from Eurofins Genomics.
Cathepsin B primer sequences:
Forward primer (5'->3'): CTC TGA CCG GAT CTG CAT C
Reverse primer (5'->3'): TCA CAG GGA GGG ATG GAG TA

Protein extraction and western blot analysis
4×10^5 A375, 7.5×10^5 C32 and UACC62, 5×10^5 501 Mel, 6.5×10^5 SK-Mel-5 and SK-Mel-28 cells were seeded in p60 plates. As reported in[5], pellets were resuspended in 30 μl of lysis buffer (50 mM Tris-HCl, 1% TritonX100, 0.25% NaDeoxicholate, 1 mM PMSF, 2 mM Orthovanadate, proteinase inhibitor cocktail). The mixture was incubated for 30 min on ice, then sonicated for 30 min and finally centrifuged at 14000 rpm for 30 min at 4 °C. The supernatant was then quantified using Bradford reagent and the absorbance was read at 590 nm. The samples were heated for 5 min at 95 °C, separated on 10% SDS-polyacrylamide gels (Mini-PROTEAN Precast gel, Bio-Rad) and electrotransferred to polyvinylidene difluoride (PVDF) membranes using Trans-Blot Turbo system (Bio-Rad). Membranes were blocked at room temperature for 2 h using 3% BSA in TBST for the detection of Cathepsin B or 3% milk in TBST for the detection

of GAPDH. They were then incubated ON at 4 °C with the following primary antibodies: anti-Cathepsin B rabbit monoclonal antibody (#31718, Cell Signaling Technology, dilution 1:1000 in 3% milk in TBST); anti-GAPDH rabbit polyclonal antibody (#2118, Cell Signaling Technology, dilution 1:3000 in 3% milk in TBST). The detection of primary antibodies was performed using alkaline phosphatase-conjugated secondary antibodies and enhanced chemiluminescence reagents (Clarity Western ECL Substrate, Bio-Rad).

Growth curve assay with increasing concentrations of dox, az-dox, and az-VC-dox
Growth curve assays were performed as described in [11]. Briefly, $3x10^3$ A375 cells and $1.5x10^4$ SK-Mel-28 cells were seeded in 12-well plates (2 wells per drug concentration) and 24h later they were treated with different concentrations of the appropriate drug for a week. Cells were then fixed with 2% PFA and stained with crystal violet solution (0.1% crystal violet and 20% methanol in water). After the excess crystal violet solution was removed, the plates were washed with tap water and dried, then cells were de-stained using a 10% acetic acid solution. Absorbance of the resulting solution was read at 590 nm. Each sample was normalized on the vehicle-treated sample and the data were graphed as variation of cell percentage compared with samples treated with DMSO vehicle.

Extraction of doxorubicin from the cell wall of dox-Lm^{at}/dox-VC-Lm^{at} and quantification
$4x10^8$CFU bacteria were centrifuged (7650 xg for 20 min at 4°C) and resuspended in 500 μl of chilled TE buffer (50 mM Tris-HCl, 1 mM EDTA, pH 8) containing 1 mM PMSF. This step was repeated twice. The bacterial pellet was then resuspended in 170 μl of ice-cold mutanolysin/lysozyme mix and incubated for 2h at 37°C in a shaking incubator.
To obtain 1 mL of the mutanolysin/lysozyme mix in TES buffer (TES buffer is TE buffer with 20% (v/w) sucrose): 50 μl of 5.000 U/mL mutanolysin solution (Mutanolysin from Streptomyces globisporus, Sigma-Aldrich, #M9901), freshly prepared in chilled and filter-sterilized 0,1 M K_2HPO_4 solution at pH 6.2; 100 μL of 100 mg/ml lysozyme solution (Sigma-Aldrich), freshly prepared in TES buffer.
After incubation, the enzymatically digested bacteria were centrifuged at 14.000 xg for 5 min and the supernatant was collected. The amount of doxorubicin present in the supernatant was estimated by fluorescence measurement with Tecan Infinite M200 Pro plate reader (Ex480/Em590). To this end, a calibration curve composed of fourteen concentrations of doxorubicin, starting from 8 μM and performing a 1:2 serial dilution, were used.

Test of Cathepsins-mediated release of doxorubicin from dox-VC-Lm^{at}
Once SK-Mel-28 cell lysate was obtained as described above (see *Cleavage of azido-VC-dox using SK-Mel-28 cell lysate*), the pH was adjusted 8 by adding 0,2 M NaOH if needed, or it was acidified to 4 by adding 0,2M HCl. Acidic pH is necessary to activate cytoplasmic Cathepsins and promote the cleavage of the Valine-Citrulline dipeptide. Then, $4x10^8$ CFU of dox-VC-Lm^{at} were incubated in the lysate ON at 37°C. Further control samples included in the experiment were: lysate alone, lysate + 1 μM dox, lysate + $4x10^8$ CFU unloaded Lm^{at}, lysate + 1 μM dox + $4x10^8$ CFU Lm^{at}. Subsequently, the mixture was filtered with 3K and then 0,22 μM spin columns filters, to remove cellular debris as well as to make the solution sterile. Finally, two volumes of complete DMEM medium were added to one volume of supernatant and the pH was adjusted to 8, adding 0,2 M NaOH if needed. Activated lysate was added to SK-Mel-28 cells, seeded the day before at $3x10^3$ cells/96 well plate. After 48h of incubation, cells were fixed with NOTOXhisto, according to the manufacturer's protocol, and stained with 300nM DAPI. Cells nuclei where then counted by fluorescent microscopy. 3 fields per well were visualized with Nikon EclipseTi2 fluorescent microscope equipped with a Nikon camera (Nikon NIS Elements software), 20x objective.

REFERENCES

(1) Liechti, G. W.; Kuru, E.; Hall, E.; Kalinda, A.; Brun, Y. V.; VanNieuwenhze, M.; Maurelli, A. T. A New Metabolic Cell-Wall Labelling Method Reveals Peptidoglycan in Chlamydia Trachomatis. *Nature* **2014**, *506* (7489), 507–510. https://doi.org/10.1038/nature12892.

(2) Vitiello, M.; Evangelista, M.; Di Lascio, N.; Kusmic, C.; Massa, A.; Orso, F.; Sarti, S.; Marranci, A.; Rodzik, K.; Germelli, L.; Chandra, D.; Salvetti, A.; Pucci, A.; Taverna, D.; Faita, F.; Gravekamp, C.; Poliseno, L. Antitumoral Effects of Attenuated Listeria Monocytogenes in a Genetically Engineered Mouse Model of Melanoma. *Oncogene* **2019**, *38* (19), 3756–3762. https://doi.org/10.1038/s41388-019-0681-1.

(3) Kim, S. H.; Castro, F.; Gonzalez, D.; Maciag, P. C.; Paterson, Y.; Gravekamp, C. Mage-b Vaccine Delivered by Recombinant Listeria Monocytogenes Is Highly Effective against Breast Cancer Metastases. *Br J Cancer* **2008**, *99* (5), 741–749. https://doi.org/10.1038/sj.bjc.6604526.

(4) Siegrist, M. S.; Whiteside, S.; Jewett, J. C.; Aditham, A.; Cava, F.; Bertozzi, C. R. (D)-Amino Acid Chemical Reporters Reveal Peptidoglycan Dynamics of an Intracellular Pathogen. *ACS Chem Biol* **2013**, *8* (3), 500–505. https://doi.org/10.1021/cb3004995.

(5) Kimmel, C. B.; Ballard, W. W.; Kimmel, S. R.; Ullmann, B.; Schilling, T. F. Stages of Embryonic Development of the Zebrafish. *Developmental Dynamics* **1995**, *203* (3), 253–310. https://doi.org/10.1002/aja.1002030302.

(6) Marranci, A.; Jiang, Z.; Vitiello, M.; Guzzolino, E.; Comelli, L.; Sarti, S.; Lubrano, S.; Franchin, C.; Echevarría-Vargas, I.; Tuccoli, A.; Mercatanti, A.; Evangelista, M.; Sportoletti, P.; Cozza, G.; Luzi, E.; Capobianco, E.; Villanueva, J.; Arrigoni, G.; Signore, G.; Rocchiccioli, S.; Pitto, L.; Tsinoremas, N.; Poliseno, L. The Landscape of BRAF Transcript and Protein Variants in Human Cancer. *Mol Cancer* **2017**, *16* (1). https://doi.org/10.1186/s12943-017-0645-4.

(7) Marranci, A.; Prantera, A.; Masotti, S.; De Paolo, R.; Baldanzi, C.; Podda, M. S.; Mero, S.; Vitiello, M.; Franchin, C.; Laezza, M.; Comelli, L.; Arrigoni, G.; Cervelli, T.; Del Pozzo, G.; Poliseno, L. PARP1 Negatively Regulates MAPK Signaling by Impairing BRAF-X1 Translation. *J Hematol Oncol* **2023**, *16* (1), 33. https://doi.org/10.1186/s13045-023-01428-2.

(8) Pham, L. N.; Kanther, M.; Semova, I.; Rawls, J. F. Methods for Generating and Colonizing Gnotobiotic Zebrafish. *Nat Protoc* **2008**, *3* (12), 1862–1875. https://doi.org/10.1038/nprot.2008.186.

(9) Pietrobono, S.; De Paolo, R.; Mangiameli, D.; Marranci, A.; Battisti, I.; Franchin, C.; Arrigoni, G.; Melisi, D.; Poliseno, L.; Stecca, B. P38 MAPK-Dependent Phosphorylation of Transcription Factor SOX2 Promotes an Adaptive Response to BRAF Inhibitors in Melanoma Cells. *Journal of Biological Chemistry* **2022**, *298* (9), 102353. https://doi.org/10.1016/j.jbc.2022.102353.

(10) Vitiello, M.; Tuccoli, A.; D'Aurizio, R.; Sarti, S.; Giannecchini, L.; Lubrano, S.; Marranci, A.; Evangelista, M.; Peppicelli, S.; Ippolito, C.; Barravecchia, I.; Guzzolino, E.; Montagnani, V.; Gowen, M.; Mercoledi, E.; Mercatanti, A.; Comelli, L.; Gurrieri, S.; Wu, L. W.; Ope, O.; Flaherty, K.; Boland, G. M.; Hammond, M. R.; Kwong, L.; Chiariello, M.; Stecca, B.; Zhang, G.; Salvetti, A.; Angeloni, D.; Pitto, L.; Calorini, L.; Chiorino, G.; Pellegrini, M.; Herlyn, M.; Osman, I.; Poliseno, L. Context-Dependent MiR-204 and MiR-211 Affect the Biological Properties of Amelanotic and Melanotic Melanoma Cells. *Oncotarget* **2017**, *8* (15). https://doi.org/10.18632/oncotarget.15915.

(11) Vitiello, M.; Evangelista, M.; Zhang, Y.; Salmena, L.; Pandolfi, P. P.; Poliseno, L. PTENP1 Is a CeRNA for PTEN: It's CRISPR Clear. *J Hematol Oncol* **2020**, *13* (1). https://doi.org/10.1186/s13045-020-00894-2.